Examining the Role of DNM1L-Dependent Mitochondrial Fission and Mitophagy Receptors During Skeletal Muscle Differentiation

by

Andrew Sing Fai Ma

A thesis

presented to the University of Waterloo

in fulfilment of the

thesis requirement for the degree of

Master of Science

in

Kinesiology

Waterloo, Ontario, Canada, 2020

Author's Declaration

I hereby declare that I am the sole author of this thesis. This is a true copy of the thesis, including any required final revisions, as accepted by my examiners.

I understand that my thesis may be made electronically available to the public.

Abstract

Mitochondrial fission is necessary for the remodelling of existing mitochondria during skeletal muscle differentiation. When there is a need for muscle regeneration or repair, stem cell-like myoblasts exit the cell cycle, restructure their mitochondrial networks, and fuse together to form multinucleated myotubes. Studies investigating the cellular process of DNM1L (dynamin 1-like)-dependent mitochondrial fission during skeletal muscle differentiation are limited. Here, we demonstrated the effect of DNM1L inhibition with mdivi-1 (mitochondrial division inhibitor-1), a pharmacological inhibitor of DNM1L self-assembly, during murine C2C12 myoblast differentiation. Myoblasts treated with mdivi-1 exhibited a hyperfused mitochondrial network which consisted of increased branch lengths and inversely decreased the number of mitochondrial puncta, suggesting the reduction of DNM1L-driven mitochondrial fission events. Furthermore, inadequate mitochondrial fission suppressed MYH (myosin heavy chain) levels and concomitantly decreased myoblast cell fusion during myotube formation. To further support the notion that DNM1L is required for myoblast differentiation, we attempted to genetically knockdown *Dnm1l* expression with a short hairpin RNA which marginally decreased DNM1L protein content and dramatically abolished MYH levels. In contrast, DNM1L overexpression in differentiated myoblasts did not impair MYH levels. Moreover, we examined the effect of excess mitochondrial fission with CCCP (carbonyl cyanide 3-chlorophenylhydrazone), a chemical inducer of mitochondrial depolarization, which promoted MAP1LC3B (microtubule associated protein 1 light chain 3 beta) conversion indicating that CCCP stimulated autophagy, an intracellular degradation system for the removal of proteins and organelles. Previous studies demonstrated the

importance for the degradation of mitochondria facilitated by the mitophagy receptors BNIP3 (BCL2 interacting protein 3) and PRKN (parkin RBR E3 ubiquitin protein ligase) but overlooked the relation of DNM1L during skeletal muscle differentiation. In this study, we examined the mitophagy-related proteins BNIP3 and PRKN in the context of DNM1L inhibition during myoblast differentiation. Importantly, mdivi-1 treated myoblasts overexpressed with BNIP3 ameliorated myoblast cell fusion and upregulated MYH, whereas PRKN overexpression ineffectively restored myotube formation. Collectively, our findings further support the integral role of DNM1L in the process of mitochondrial fission, as well as emphasize the interplay between DNM1L and mitophagy receptors during C2C12 myoblast differentiation.

Acknowledgements

A sincere thank you to my supervisor, Dr. Joe Quadrilatero, for your mentorship and expertise throughout my master's degree. I am grateful for the numerous learning opportunities, access to equipment, and collaborative research projects, that you have provided. I appreciate the years of experience under your supervision building a repertoire of skills and laboratory techniques like performing animal studies, mammalian cell culture, bacterial culture, and adenovirus amplification. Thank you to my committee members, Dr. Robin Duncan and Dr. Michaela Devries-Aboud, for your time and critical suggestions in the implementation of this study. Your insight and thorough evaluation of the experiments ensured that the projects were attainable. I must also extend my gratitude to my past and current coworkers. Each of you made my experience in the Quad Squad even better. A heartfelt thank you to Fatemeh K. for your patience, understanding, and kindness; Rishiga P. for your generosity and encouragement; and James T. for your cheerfulness and support. Thank you to Dr. Bruce Reed and Dr. Brittany Baechler for starting my career in the sciences. I gained invaluable knowledge and professional training from the Developmental Biology and Genetics Lab that proved useful in the Muscle Biology and Cell Death Lab. Thank you to external researchers Hashim I. and Jacob B. from Queen's University for allowing me to do what I do best—fluorescent microscopy techniques; and thank you to Dr. Anderson Zago and Ana P. for enriching my master's experience. Finally, thank you to my parents and my sister for your love, support, and the sacrifices that you made while I was away from home. To my grandparents, thank you for letting me stay during this pandemic while I wrote my thesis.

Table of Contents

List of Figures

List of Illustrations

List of Abbreviations

ATG	autophagy-related (protein)
BAX	BCL2-associated X, apoptosis regulator
BCL2	BCL2 apoptosis regulator
BECN1	beclin 1
BNIP3	BCL2 interacting protein 3
BNIP3L (NIX)	BCL2 interacting protein 3-like
C2C12	murine myoblast cell type
CCCP	carbonyl cyanide 3-chlorophenylhydrazone
DNM1L	dynamin 1-like
GAPDH	glyceraldehyde-3-phosphate dehydrogenase
GFP	green fluorescent protein
MAP1LC3B (LC3B)	microtubule-associated protein 1 light chain 3 beta
LC3B-II	MAP1LC3B conjugated to phosphatidylethanolamine
Mdivi-1	mitochondrial division inhibitor-1
MFN2	mitofusin 2
MYH	myosin heavy chain
MYOG	myogenin
p-H2AFX	phosphorylated H2A histone family, member X
PINK1	PTEN induced kinase 1
PRKN	parkin RBR E3 ubiquitin protein ligase

1.0 Introduction

A population of myogenic precursor cells, hereafter called myoblasts, reside in skeletal muscle and their activation may have therapeutic potential in response to muscle damage and tissue repair [1]. Myogenesis is a process in which myoblasts differentiate and mature into multinucleated myotubes. While myoblasts manifest a glycolytic phenotype [2], the coordination of several processes governing the remodelling of the mitochondrial network such as the mitochondrial dynamics of fission and fusion, the degradation of existing mitochondria, and the biogenesis of new mitochondria, increase the capacity for mitochondrial oxidative phosphorylation in myoblasts during myotube formation [2], [3].

Mitochondria are dynamic organelles that constantly fuse, divide, and remodel their structures. Mitochondrial fission is the division of a mitochondrion into distinct mitochondria and this is executed by a master fission mediator, DNM1L protein (DRP1, dynamin 1-like) [4], [5]. Conversely, mitochondrial fusion is the amalgamation of adjacent mitochondria and this is induced by OPA1 protein (OPA1 mitochondrial dynamin like GTPase) localized on the inner mitochondrial membrane and by proteins MFN1 and MFN2 (mitofusin 1, mitofusin 2) inserted into the outer mitochondrial membrane [4], [5]. Mitochondria form an interconnected network and increasing evidence suggest that changes in the organization of mitochondria affect the cellular mechanisms of cell survival, cell death, and cell differentiation [6]–[8].

Autophagy is a degradative process that recycles proteins and organelles [9]. A facet of this degradation pathway is the elimination of mitochondria called mitophagy [10]. Mitophagy segregates and degrades a mitochondrion from the existing

mitochondrial network. The importance of mitophagy in myoblasts was noted in the absence of key mitophagy proteins such as BNIP3 (BCL2 interacting protein 3) and PRKN (parkin RBR E3 ubiquitin protein ligase) [11]–[13]. Mitochondria play a crucial role in the maintenance of energy balance and the preservation of cell viability, since dysregulation of mitochondrial dynamics or impaired autophagy/mitophagy, elicits the activation of programmed cell death [14]–[16].

Previous studies highlighted the importance for DNM1L-mediated mitochondrial fission during myogenesis [7], [17], while other studies demonstrated that mitophagy was necessary for myogenic differentiation [2], [11]; however, few studies have examined the effect of DNM1L inhibition and the influence of BNIP3 and PRKN mitophagy receptors during C2C12 myoblast differentiation. We utilized a selective pharmacological inhibitor of DNM1L GTPase activity, mitochondrial division inhibitor-1 (mdivi-1), and a short hairpin RNA against *Dnm1l* to further elucidate the role of DNM1L during C2C12 myoblast differentiation. Despite a previous study [7] demonstrated the effect of mdivi-1 on myoblast differentiation, the levels of BNIP3 and PRKN were not evaluated in this context. Since DNM1L, BNIP3, and PRKN participate in the process of mitochondrial network remodelling, we postulated that the overexpression of BNIP3 or PRKN in mdivi-1 treated myoblasts would restore myotube formation. Therefore, in the current study we examined the role of DNM1L and investigated the effect of mitophagy receptors BNIP3 and PRKN in mdivi-1 treated myoblasts during myogenic differentiation.

1.1 General Autophagy

Autophagy is a catabolic mechanism for the bulk degradation of cellular cargo enclosed by double-membraned autophagosomes [18]. The removal of cytosolic material is an evolutionarily conserved eukaryotic process mediated by ATG (autophagy-related) proteins that subsequently lead to the fusion of autophagosomes with lysosomes to degrade cytosolic substrates [14], [19]–[21]. Under normal conditions, basal level of autophagy is generally low, and the activation of autophagy promotes the turnover of existing cellular structures [22]. Lysosomal acid hydrolases degrade lipids, proteins, and DNA into components that can later contribute to the formation of new membranes, participate in protein synthesis, or provide nutrients and metabolites [22].

Autophagosome Membrane Formation

The formation of the autophagosome membrane is controlled by an upstream protein complex composed of ULK1 (unc-51 like autophagy activating kinase 1), ATG13, and FIP200 (focal adhesion kinase family-interacting protein of 200 kDa/ RB1CC1) [18], [22], [23]. Normally mTOR-C1 (mammalian target of rapamycin-complex 1) suppresses autophagy in nutrient rich conditions by phosphorylating ULK1 and ATG13 [24]–[27]. During starvation, mTOR-C1 dissociates from the ULK complex initiating autophagy and decreases protein synthesis (**Illustration 1a**). The assembly of the autophagosome membrane requires a phosphatidylinositol 3-kinase (PIK3) complex, which is composed of PIK3C3 (PIK3 catalytic subunit type 3/VPS34), ATG14, and BECN1 (beclin 1) [28]–[31]. In the absence of autophagy, anti-apoptotic protein BCL2 (BCL2 apoptosis regulator) inhibits autophagy by interacting with BECN1. The dissociation of BECN1 from BCL2 is required for autophagy induction [15].

Subsequently, the PIK3 complex and several ATG proteins recruit two ubiquitin-like conjugation systems to the autophagosome membrane: (1) ATG5-ATG12-ATG16 and (2) MAP1LC3B/LC3B (microtubule-associated protein 1 light chain 3 beta)-conjugated to PE (phosphatidylethanolamine, **Illustration 1b**) [22], [32], [33]. Briefly, a upstream E1-like enzyme ATG7 activates ATG12, then ATG10, an E2-like enzyme, conjugates ATG12 to ATG5 (**Illustration 1c**). ATG7 also activates LC3B-I, then ATG3 conjugates phospholipid PE to LC3B-I which converts LC3B-I to LC3B-II. After the autophagosome encloses its cargo, the ATG5-ATG12-ATG16 complex dissociates from the outer membrane leaving LC3B-II tethered to the inside of the autophagosome. Next, LAMP2 (lysosome-associated membrane protein 2) and the small GTPase RAB7A (RAB7A, member RAS oncogene family) fuses the autophagosome with a lysosome [22], [34], [35].

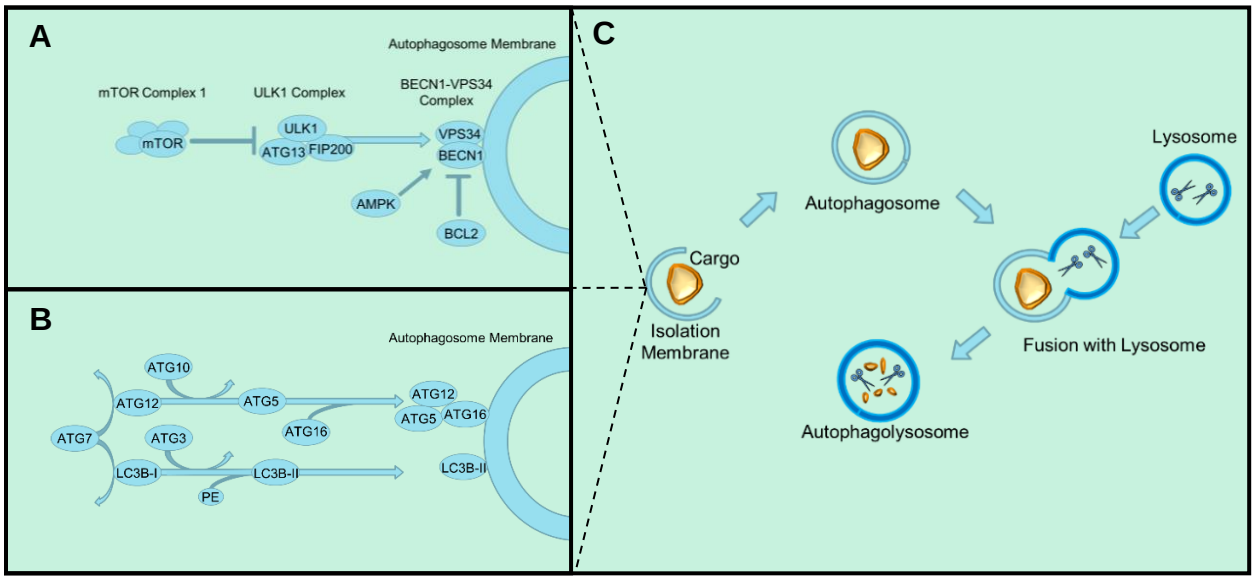

Illustration 1. Flow diagram summarizing the process of autophagy.
(**a**) mTOR inhibition of the ULK1 complex prevents autophagosome formation. The ULK1 complex recruits the BECN1-VPS34 complex to the isolation membrane. (**b**) ATG7 activates both the ATG5-ATG12-ATG16 conjugation system and the LC3B-phosphatidylethanolamine (PE) conjugation system during autophagosome membrane elongation. (**c**) Cytosolic and organellar cargo are enveloped by a double-membraned autophagosome which then fuses with a lysosome.

Cargo Recognition by Autophagy Receptors Tethered to the Autophagosome

SQSTM1 (sequestosome 1) [22], [36]–[38] is an autophagy-associated protein with a ubiquitin domain that binds to ubiquitinated cytosolic and membrane-bound proteins identified for proteolysis. Unlike the ubiquitin-proteasome system (UPS) where ubiquitinated proteins are degraded by this mechanism, organellar structures and large portions of the cytosol are removed via autophagy. SQSTM1 contains a LC3B-II interacting region (LIR) that tethers ubiquitinated cargo to the inside of the autophagosome. Functionally like SQSTM1, NBR1 protein (NBR1 autophagy cargo receptor) and OPTN protein (optineurin) both contain LIR and ubiquitin binding domains. Moreover, AMBRA1 (autophagy and beclin 1 regulator 1) is another autophagy protein that interacts with LC3B-II [39]. This exemplifies the redundant autophagy proteins that promote the recognition of cargo by the autophagosome.

1.2 Selective Autophagy of Mitochondria is Called Mitophagy

The selective autophagy of organelles was shown by the degradation of the endoplasmic reticulum [21], peroxisomes [40], and mitochondria [41], [42]. In the context of programmed mitochondrial degradation termed *mitophagy*, three developmental cellular models for the targeted removal of mitochondria have been identified: (1) the elimination of paternal mitochondria during fertilization of the zygote [43], (2) the development of the ocular lens [44], and (3) the maturation of erythrocytes [45]–[47]. Mitophagy receptors identify mitochondria for degradation including mitochondria with depolarized membrane potential [5], [14], [39], [48]–[51]. Localized on the outer mitochondrial membrane (OMM), mitophagy receptors interact with ubiquitin-SQSTM1 or LC3B-II tethered to the inner membrane of the autophagosome.

Several mitophagy receptor acting independently or concomitantly have been characterized such as BNIP3, BNIP3L/NIX, PINK1, and PRKN [46], [50], [52]–[54]. Given that autophagy is required for normal muscle development, mitophagy may also promote cell viability when there exists mitochondria with decreased membrane potential or when there is a need to eliminate unnecessary mitochondria, in particular, during the process of myoblast differentiation [3], [42].

BNIP3 and BNIP3L/NIX Mitophagy Receptors

The mitophagy receptors BNIP3 (BCL2 interacting protein 3) and its homologue BNIP3L/NIX (BCL2 interacting protein 3-like) mediate the selective removal of mitochondria. BNIP3 is a BCL2 homology domain 3 (BH3)-only protein that homodimerizes on the OMM by its *C*-terminus transmembrane domain (TM) and contains a *N*-terminus LC3B-II interacting region to promote the formation of autophagosomes around mitochondria [21], [39], [55]. BNIP3-TM domain mutants ($BNIP3^{G180F}$ or $BNIP3^{H173A}$) abrogates homodimerization and reduces mitophagy [21], [39], [55] as demonstrated in HeLa cells through fluorescent microscopy for co-localized GFP-LC3-positive autophagosomes [21]. Overexpression of the wildtype BNIP3 increased the number of mitophagy-positive cells, supporting that BNIP3 was involved in mitophagy. Furthermore, immunoblot analysis confirmed increased endogenous LC3B-II levels in HeLa cells overexpressing BNIP3, but not for BNIP3-TM mutants [21]. Moreover, a mutation in the conserved LIR motif ($BNIP3^{W18A}$) abolished the interaction of BNIP3 with LC3B-II and reduced mitophagy [21]. Thus, BNIP3 TM domain or LIR domain mutations impeded BNIP3-induced degradation of mitochondria.

PINK1 and PRKN Mitophagy Receptors

The mitophagy receptor PINK1 (PTEN-induced kinase 1) accumulates on the OMM of depolarized mitochondria [14], [39], [48]–[51]. Functionally, PINK1 may be a sensor for the polarization state of mitochondria. PINK1 is normally cleaved in the intermembrane space by PARL (protease presenilin-associated rhomboid-like) and by the proteasome in the cytosol [39], [56], [57]. In response to decreased mitochondrial membrane potential, PINK1 remains intact and accumulates on the OMM which recruits cytosolic PRKN (parkin RBR E3 ubiquitin protein ligase). Mutations in PRKN manifests pathological symptoms of Parkinson's Disease [58], [59]. Narendra *et al.* (2008) demonstrated that PRKN played a vital role during mitophagy in mammalian cells [60]. Currently, it is unknown how PRKN is recruited to PINK1 but the phosphorylation of ubiquitinated proteins by PINK1 and the ubiquitination of other OMM proteins appear to translocate PRKN from the cytosol to the mitochondria [61]–[63].

1.3 Mitochondrial Fission-Fusion Dynamics and Mitophagy

Mitophagy facilitates the removal of damaged mitochondria and maintains the quality of the mitochondrial network [64], [65]. In a metabolically active tissue like skeletal muscle, mitophagy is critical for mitochondrial homeostasis since mitochondria maintain energy balance and are large producers of reactive oxygen species [64]. It has been suggested that the architecture of the mitochondrial network contributes to the bioenergetics of mitochondria through mitochondrial dynamics of continuous fission and fusion events [66].

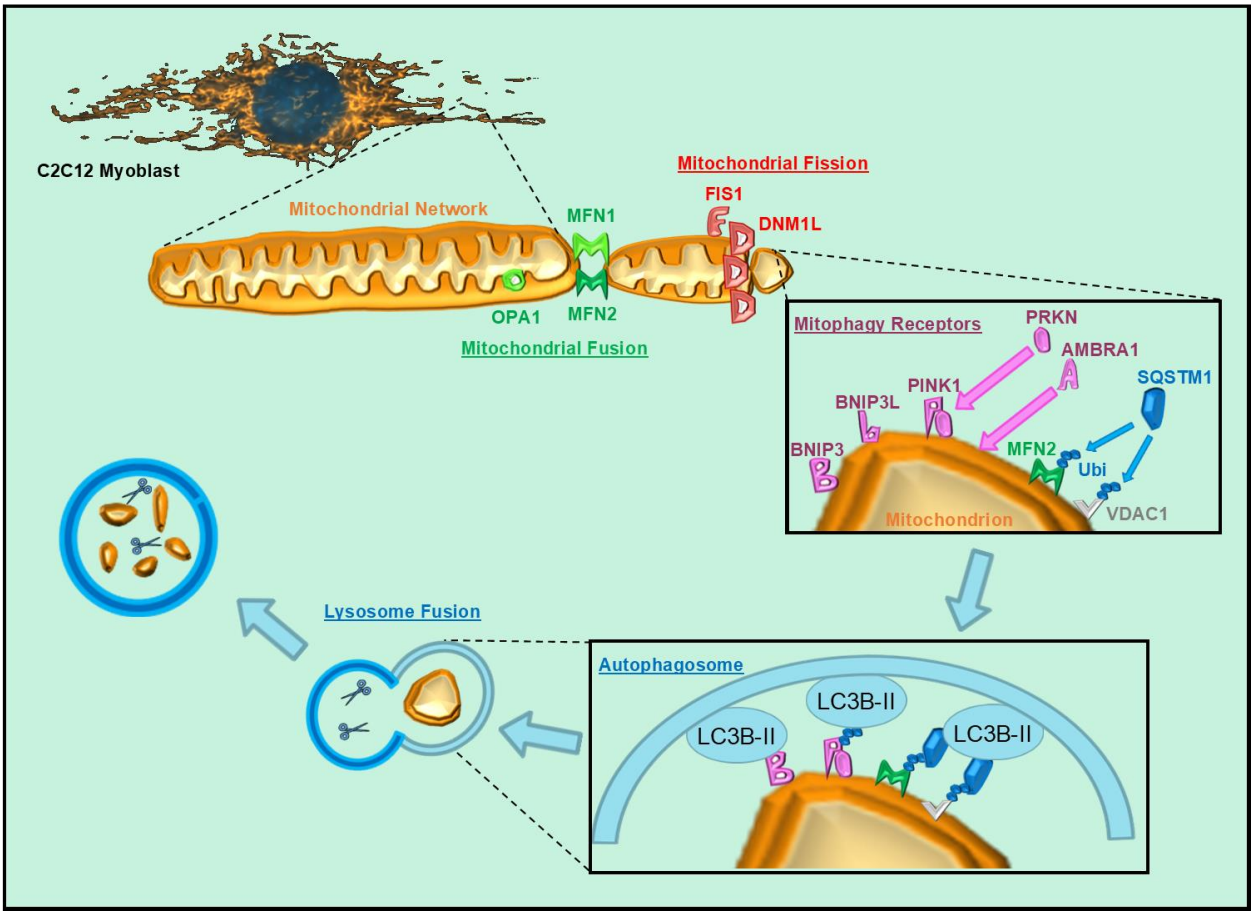

Illustration 2. A detailed flow diagram of the interactions between proteins governing the processes of mitochondrial dynamics and mitophagy. Mitochondrial fission proteins (DNM1L, FIS1) and mitochondrial fusion proteins (OPA1, MFN1, MFN2) are involved in the remodelling of the mitochondrial network. Furthermore, the mitophagy receptors (BNIP3, BNIP3L/NIX, PINK1, PRKN, AMBRA1) enable the recognition of mitochondria by autophagy proteins (SQSTM1, LC3B-II). Outer mitochondrial membrane proteins (VDAC1, MFN1, MFN2) are ubiquitinated (Ubi) and targeted for degradation by the ubiquitin-proteasome system and the mitochondrion is enveloped by the autophagosome.

The interplay between mitochondrial dynamics and mitophagy appear to influence the overall function of mitochondria and the cellular processes of respiration, differentiation, and apoptosis [67]–[69]. A family of dynamin-related GTPases participate in the mitochondrial dynamics of fission and fusion. Mitochondrial fission is the partitioning of a mitochondrion into two daughter mitochondria. The main inducer of

mitochondrial fission is DNM1L (dynamin 1-like) which is recruited by FIS1 (fission, mitochondrial 1). Conversely, mitochondrial fusion is the merging of the mitochondrial membranes of two adjacent mitochondria and this is induced by OPA1 (OPA1 mitochondrial dynamin like GTPase) located on the inner mitochondrial membrane and by MFN1 and MFN2 (mitofusins-1 and -2) which are inserted onto the OMM [8], [70]–[74] (**Illustration 2**).

Mitochondrial Fusion Events with MFN1, MFN2, OPA1

MFN1 and MFN2 are large GTPases that promote the initial step of mitochondrial fusion and lead to the elongation of mitochondria [75]. MFN2 is also involved in controlling mitochondrial metabolism [4], [76] and tethering mitochondria to the endoplasmic reticulum [77]. It appears that PINK1-dependent phosphorylation of MFN2 at Ser442 and Thr111 recruits PRKN [78]–[81] to prevent the re-fusion of defective mitochondria with the existing mitochondrial network.

OPA1 regulates the fusion of the inner mitochondrial membranes but a study suggested that OPA1 may also alter cristae structure [71]. YME1L (mitochondrial protease yeast mitochondria escape-1-like) cleaves OPA1 in mitochondria with depolarized membranes or depleted of ATP, which may prevent dysfunctional mitochondria from participating in subsequent fusion events [4], [8], [70], [82]. Mutations in the GTPase domain of OPA1 impairs its pro-fusion activity and leads to CYCS (cytochrome c) release from the mitochondrial intermembrane space to the cytosol, a hallmark of activated mitochondrial apoptosis. Mitochondrial fusion events appear to play a critical role in the exchange of mitochondrial matrix and inner mitochondrial membrane proteins between mitochondria [83].

Mitochondrial Fission Events with FIS1 and DNM1L

Mitochondrial fission generates a subpopulation of non-fusing mitochondria with reduced membrane potential and decreased OPA1 levels to facilitate their removal by mitophagy [4], [9]. Knockdown of FIS1 by silencing RNA in pancreatic *b*-cells treated with high glucose and fatty acid prevented the recruitment of DNM1L to the mitochondria, decreased the number of autophagosomes containing mitochondria, and enabled the exchange of mitochondrial components through net mitochondrial fusion events [8]. In starved mice, knockdown of FIS1 expression resulted in retained muscle and mitochondrial mass, prevented mitochondrial fragmentation, and decreased autophagy [84]. This highlights the cooperativity of mitochondrial fission proteins and the downstream effects of mitochondrial fission on autophagy. Since mitophagy receptors were not measured in the mentioned studies, this warrants further examination of the mechanisms that govern mitophagy and mitochondrial fission and fusion in the context of muscle regeneration.

Recently the mitochondrial fission protein DNM1L received growing attention for its role in myogenic differentiation. It was determined by immunoblot that DNM1L levels transiently increased early in the differentiation process [17]. Mitochondrial-enriched fractions obtained after subcellular fractionation indicated that DNM1L content increased during C2C12 myoblast differentiation [7]. Mitochondrial division inhibitor-1 (mdivi-1), a selective chemical inhibitor of DNM1L GTPase activity, suppressed myogenic differentiation as the number of multinucleated MYH (myosin heavy chain)-positive cells decreased in a dose-dependent manner [7]. Thus, DNM1L presents a relevant function in the progression of skeletal muscle differentiation.

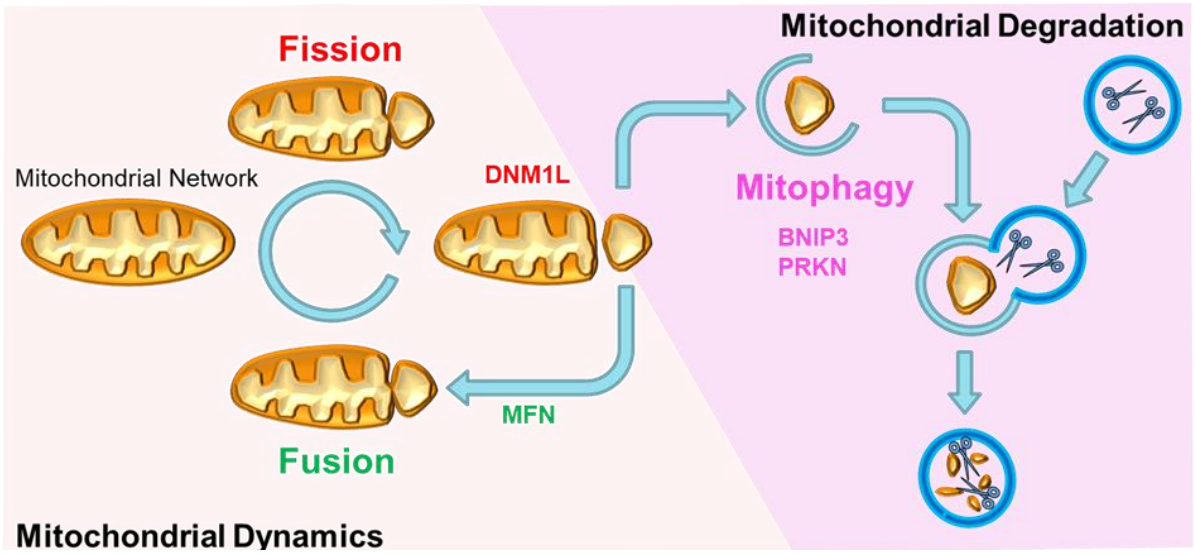

Illustration 3. Conceptual representation of the interplay between the processes of mitochondrial dynamics and mitophagy.

The mechanisms regulating mitochondrial morphology are integrated with the mitophagy program. One theory postulates that mitochondrial fission events separate mitochondria from the existing mitochondrial network and these mitochondria are eliminated by mitophagy [8], [52], [66]. It was shown that mitochondria are targeted for autophagy by increasing the ubiquitination of OMM integral proteins such as MFN1, MFN2, TOM (translocase of the outer membrane), VDAC1 (voltage dependent anion channel 1) [80], [85]–[87]. Furthermore, PINK1/PRKN-mediated mitophagy in MFN knockout cells may be assisted by other mitophagy receptors. Zhang *et al*. [88] demonstrated in HEK cells that BNIP3 interacted with PINK1 and cooperatively promoted the insertion of full-length PINK1 onto the OMM. Inactivation of BNIP3 through a mutation in the TM domain exacerbated the proteolysis of PINK1 and resulted in the suppression of PINK1/PRKN-mediated mitophagy [88].

Thus, a link between mitochondrial dynamics and mitophagy may regulate the morphology of the mitochondrial network in skeletal muscle. Functional mitochondria

can continue to participate in fusion events, but mitophagy may target any depolarized or dysfunctional mitochondria (**Illustration 3**). Consistent with these observations reported in other cell types, inhibiting the mitochondrial fission proteins or enhancing mitochondrial fusion both decreased mitophagy [76], [83], [89], while augmenting mitochondrial fission promoted mitophagy [39], [52], [69]. Hence, further studies elucidating the interplay of mitochondrial dynamics and mitophagy in the context of myogenic differentiation warrant further investigation.

1.4 Crosstalk Between Mitochondrial Fission and Mitophagy in Skeletal Muscle Differentiation

Skeletal muscle cells are terminally differentiated myofibres. Skeletal muscle differentiation is the process whereby a population of mononucleated stem cell-like myoblasts exit the cell cycle and fuse together to form multinucleated myotubes [15], [90]. During muscle development or repair, myoblasts fuse to adjacent myoblasts or contribute their nuclei to existing myofibres. Myoblast differentiation is controlled by myogenic regulatory transcription factors (e.g. MYOG, myogenin) [91], [92]. The content of MYH (myosin heavy chain) is upregulated and the cell fusion of myoblasts are characteristics of myotube formation.

The relative rates of mitochondrial fission and fusion alter the overall morphology of mitochondria and subsequently affect the function of these organelles as regulators of energy metabolism. It was shown that blocking mitochondrial fusion increased mitochondrial network fragmentation during apoptosis [71], [93], [94]. However, enhanced mitochondrial fission alone did not induce programmed cell death [95]. Since myoblasts undergo a dramatic restructuring of their mitochondrial network during differentiation, we investigated the role of DNM1L in the process of mitochondrial fission

and the effect of DNM1L inhibition during myoblast differentiation. We also examined the effect of overexpressing mitophagy receptors BNIP3 and PRKN in DNM1L inhibited myoblasts during differentiation. One study determined that DNM1L-mediated mitochondrial fission was critical for muscle differentiation by inhibiting DNM1L with mdivi-1 [7]. However, the role of BNIP3 and PRKN during DNM1L inhibited myoblast differentiation were not investigated. Thus, we examined the levels of mitophagy receptors BNIP3 and PRKN and proposed that mitochondrial dynamics of fission cooperatively work with mitophagy receptors BNIP3 and PRKN to coordinate the necessary mitochondrial network changes for myoblast differentiation (**Illustration 4**). Therefore, we investigated the interplay between mitochondrial fission and select mitophagy receptors during myoblast differentiation.

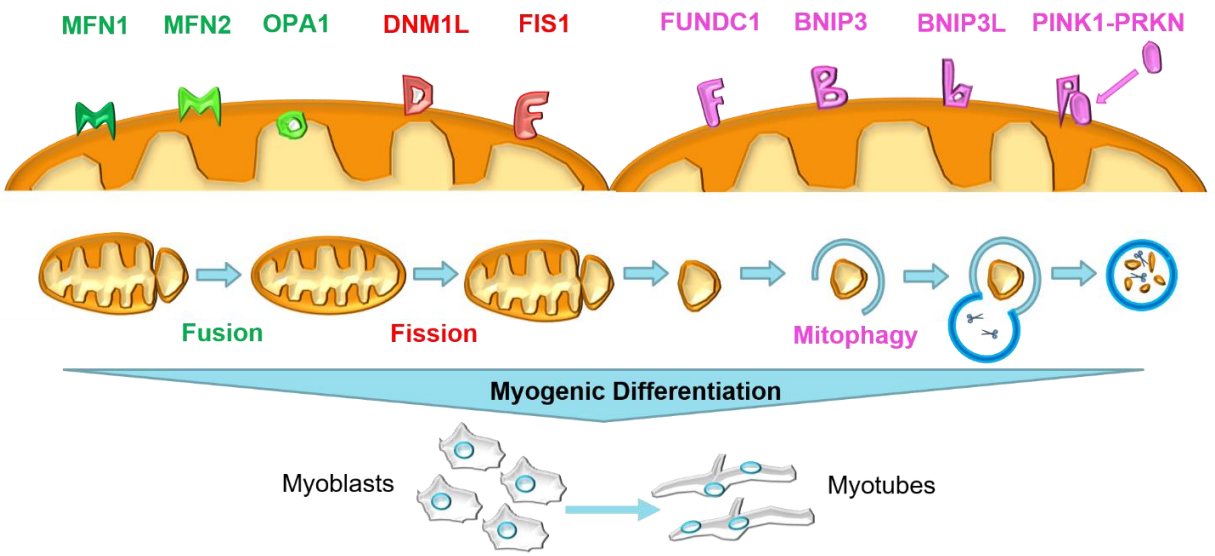

Illustration 4. Graphical summary of the relationships between mitochondrial dynamics of fusion (green), mitochondrial fission/division (red), and mitochondrial degradation/mitophagy (purple) that permit mitochondrial network remodelling during myoblast differentiation.

2.0 Research Purpose

Previous research [11] established a requirement for mitophagy in skeletal muscle differentiation and demonstrated that BNIP3-mediated mitophagy was critical for C2C12 myoblast differentiation. Moreover, emerging studies [7] suggested a prerequisite for mitochondrial fission during myoblast differentiation, but the relation of DNM1L with mitophagy receptors BNIP3 and PRKN during skeletal muscle differentiation, in particular for C2C12 myoblast differentiation, is unknown. Since a significant remodelling of the mitochondrial morphology occurs during the process of muscle differentiation, it is possible that mitochondrial fission permits the segregation of a subpopulation of mitochondria and influences the degradation of targeted mitochondria for mitophagy.

Therefore, the experiments conducted in this thesis project:

1) Characterized DNM1L content during C2C12 myoblast differentiation,

2) Determined the effect of DNM1L protein inhibition by mdivi-1 and short hairpin RNA against *Dnm1l* during myoblast differentiation, and

3) Investigated the role of BNIP3 and PRKN in response to DNM1L inhibition during the process of myoblast differentiation.

Experiment 1: Mitochondrial fission during skeletal muscle differentiation

We used an *in vitro* model of skeletal muscle differentiation to examine the mitochondrial morphology of cells. Undifferentiated mouse skeletal myoblasts (C2C12 cells) proliferated until the induction of the differentiation program with differentiation media. Cells were treated with mitochondrial division inhibitor (mdivi-1) to decrease mitochondrial fission events. Conversely, excess mitochondrial fission was induced with carbonyl cyanide 3-chlorophenylhydrazone (CCCP), a chemical depolarizer of mitochondria. Optimal chemical concentrations were previously determined by colleagues in the lab [17], [96]. Mitochondrial morphology and network branching were visualized with a mitochondrial reporter construct and fluorescent microscopy. Differentiated cells were collected from culture after various lengths of time incubated in differentiation media, from 0 hours to 5 days, and used for experimental analyses. The degree of differentiation (a measure of MYH-positive cells), was determined using fluorescent microscopy as well as immunoblotting for MYOG and MYH. In addition, several autophagy protein markers (LC3B-I, LC3B-II, SQSTM1), mitochondrial apoptotic signaling molecules (BAX and BCL2), and a DNA fragmentation marker (p-H2AFX) were assessed during the differentiation process.

Experiment 2: The role of DNM1L during skeletal muscle differentiation

The effect of mdivi-1 DNM1L inhibition on muscle differentiation has been marginally studied. As a proof-of-principle, a transient knockdown with short hairpin RNA against *Dnm1l* (ad-sh*Dnm1l*) was used to provide further evidence of the consequence of reduced DNM1L expression. Lastly, overexpression of the wild-type

DNM1L (ad-DNM1L) was performed to evaluate the effect of excess DNM1L protein during myoblast differentiation. For this experiment, C2C12 cells were transduced with an adenoviral DNM1L vector before the induction of myoblast differentiation. Cells were collected at various time points as in Experiment #1, and similar immunoblotting techniques were performed for measuring select markers of differentiation, autophagy, and apoptosis.

Experiment 3: Mitochondrial fission and mitophagy during skeletal muscle differentiation

Previous work from our lab demonstrated that BNIP3-mitophagy was required for C2C12 myoblast differentiation [11]. To study the effect of mitophagy receptors in the context of DNM1L inhibition, myoblasts were treated with mdivi-1 and collected as described in Experiment #2. Cells were transduced with an adenovirus vector to overexpress BNIP3 (ad-BNIP3). Co-transduction of ad-BNIP3 with a separate adenovirus harbouring the short hairpin RNA against *Dnm1l* (ad-sh*Dnm1l*) was also performed. To investigate the role of another mitophagy receptor, an adenovirus overexpressing PRKN (ad-PRKN) was used instead of BNIP3. Cells were immunoblotted for DNM1L, MYOG, and MYH. Furthermore, fluorescent microscopy visualized the cell morphology and the proportion of multinucleated MYH-positive cells was quantified at various time points of differentiation.

Hypotheses

It was hypothesized that:

1) Chemical inhibition of DNM1L with mdivi-1 would decrease mitochondrial fission events, whereas chemical depolarization of mitochondria with CCCP would augment mitochondrial fission. This would be demonstrated by:
    a. Mitochondria morphological changes from decreased mitochondrial fission events as demonstrated by a decline in the frequency of punctate mitochondria, increased length of mitochondrial branches, and concomitant increase of intersecting junctions. Conversely, morphological changes due to increased mitochondrial fission events would exhibit the inverse relationship, as visualized by fluorescent microscopy,
    b. Decreased total protein content of DNM1L and decreased levels of MYH in mdivi-1 treated cells, and
    c. Increased total protein content of DNM1L and increased levels of MYH in CCCP treated cells.
2) Overexpression with ad-DNM1L would improve myogenic differentiation and transient knockdown with ad-sh*Dnm1l* would impair muscle differentiation. This would be demonstrated by:
    a. Increased MYH content after ad-DNM1L treatment at the endpoint of the experiment (Day 5),
    b. Decreased MYH content with ad-sh*Dnm1l* treatment at D5,
    c. Increased DNM1L content after ad-DNM1L treatment, and
    d. Decreased DNM1L content after ad-sh*Dnm1l* treatment.

3) Overexpression of mitophagy receptors would rescue DNM1L inhibition in myoblasts during differentiation. This would be noted by:
    a. Increased mitophagy protein levels BNIP3 and PRKN, followed by increased levels of MYOG and MYH, as evidenced by immunoblotting, and
    b. Increased myoblast cell fusion and increased MYH-positive cells during myotube formation, as determined by fluorescent microscopy.

3.0 Materials and Methods

Cell Culture

Mouse C2C12 skeletal myoblasts (ATCC®, CRL1772™) were cultured in 6-, 12-, 24-well polystyrene plates (Sarstedt) with growth media (GM) consisting of low-glucose Dulbecco's Modified Eagle's Medium (DMEM; Sigma-Aldrich, D6046) containing 5% fetal bovine serum (FBS; Sigma-Aldrich, F1051), 5% Serum Plus II (Sigma-Aldrich, 14009C), 1% penicillin/streptomycin (Sigma-Aldrich, P0781) and incubated at 37°C in 5% CO_2. Cells were between the passages of 6 and 9 and counted before plating to ensure accurate seeding densities using a Z2 Coulter Counter (Beckman-Coulter). Every 1-2 days, culture plates were aspirated of GM, washed with warmed 1x phosphate buffered saline (PBS; Sigma-Aldrich, D1408), and replaced with fresh GM. Cells proliferated until they reached 70-80% confluence in which myoblast differentiation was induced by replacing GM with differentiation media (DM) consisting of DMEM supplemented with 2% horse serum (Sigma-Aldrich, H1270) and 1% penicillin/streptomycin.

Chemical Inhibition of Mitochondrial Fission and Mitochondrial Depolarization During Differentiation

Inhibition of DNM1L activity and subsequent mitochondrial fission was achieved with 20 µM mdivi-1 (Cedarlane, A14316) in DM and replaced daily for 5 days [97], [98]. Mitochondrial depolarization was induced by 2.5 µM or 30 µM CCCP (Sigma-Aldrich C2759) in DM and replaced daily. For all experiments, vehicle control cells were given DM with the equivalent chemical dilution of dimethyl sulfoxide (Veh; DMSO).

Transfections and Transductions

To investigate the mitochondrial network morphology in mdivi-1 or CCCP treated cells, transfections were performed with a pDsRed2-Mito vector generously provided by Dr. Douglas Green (St. Jude's Children's Research Hospital, Memphis, TN; [99]). Cells grown on glass coverslips coated with Cultrex basement membrane extract (Trevigen, 3432–010-01) were transfected using jetPRIME Transfection Reagent (Polyplus-transfection, 114–07) according to the manufacturer's protocol. Briefly, the pDsRed2-Mito vector was diluted in 200 µL of jetPRIME transfection buffer and subsequently incubated with 4 µL of jetPRIME transfection reagent for 10 min at room temperature. This mixture was added dropwise to 50-60% confluent cells cultured in GM and incubated for 4 h at 37°C and 5% CO_2.

For adenoviral transduction experiments, cells were incubated for 24 h with adenoviral vectors for either GFP (ad-GFP; kindly provided by Dr. Gökhan S. Hotamisligil, Harvard School of Public Health, Boston, MA; [100]), DNM1L-wildtype (ad-DNM1L, MOI 125; generously provided by Dr. Yisang Yoon, Augusta University, Augusta, GA; [101]), shRNA-*Dnm1l* (ad-sh*Dnm1l*, MOI 125; kindly gifted by Dr. Junichi Sadoshima, Rutgers University, New Jersey, NJ; [101]), BNIP3 (ad-BNIP3, MOI 100; [102]), or PRKN (ad-PRKN, MOI 75; [103]) both generously provided by Dr. Abhinav Diwan (Washington University School of Medicine, St. Louis, MO). Subsequently, cells were washed with warmed PBS and provided fresh GM for at least 2 h prior to the induction of myoblast differentiation. Cells were then collected (D0) or induced for myoblast differentiation by replacing GM with DM. Adenoviral stocks were amplified in HEK293 cells (generously provided by Dr. Robin Duncan, University of Waterloo,

Waterloo, ON) and the viral titer was determined by the Adeno-X Rapid Titer procedure (Clontech Laboratories, Inc.).

Cell Collections and Determination of Total Protein Content

For whole cell lysates, cells were collected via trypsinization (0.25% trypsin with 0.2g/L EDTA; Sigma-Aldrich, T4049) and centrifuged at 1000 x *g* prior to the addition of DM (day 0; D0) as well as at 24 h (D1), 72 h (D3), and 120 h (D5) following the induction of differentiation. As previously performed in our laboratory [15], cells were incubated with lysis buffer (BioShop, 20 mM HEPES, 10 mM NaCl, 1.5 mM $MgCl_2$, 1 mM DTT, 20% glycerol, and 0.1% Triton X-100, pH 7.4) containing protease inhibitors (Roche Applied Sciences, 04693116001) before sonicating on ice. The total protein content of cell lysates was measured by the BCA protein assay method and stored at -80°C until further analysis.

Immunoblotting

Immunoblotting was performed as previously described [11]. Briefly, equal amounts of protein from cell lysates were loaded and separated on 10–12% SDS-PAGE gels, transferred onto PVDF membranes (Bio-Rad Laboratories, 1620177), and blocked for 1 h at room temperature with 5% non-fat dry milk in tris buffered saline-Tween 20 (TBS-T; BioShop, 20 mM Tris, 137 mM NaCl, 0.1% Tween 20, pH 7.5). Membranes were incubated overnight at 4°C with primary antibodies against: BNIP3L/NIX, DNM1L, GAPDH, GFP, MAP1LC3B, (Cell Signaling Technology, 12396, 8570, 2118, 2955, 2775, respectively), BAX, BCL2, FIS1, MFN2, p-H2AFX, PINK1, PRKN, VDAC1 (Santa

Cruz Biotechnology, sc-493, sc-7382, sc-376469, sc-50331, sc-517348, sc-33796, sc-32282, sc-390996, respectively), MYH, MYOG (Developmental Studies Hybridoma Bank, MF20, F5D, respectively), ACT, BNIP3 (Sigma-Aldrich, A2066, B7931, respectively), or SQSTM1 (MBL, PM045). Membranes were then washed with TBS-T, incubated with the appropriate horseradish peroxidase (HRP)-conjugated secondary antibodies (Bio-Rad Laboratories, 1706515, 1706516) for 1 h at room temperature, washed with TBS-T, and bands visualized using ECL immunoblotting substrates (BioVision, K820-500) or Clarity ECL substrates (Bio-Rad Laboratories, 1705061) and a ChemiDoc MP Imaging System (Bio-Rad Laboratories). The approximate molecular weight for each protein was estimated using Precision Plus Protein Kaleidoscope and WesternC Standards (Bio-Rad Laboratories, 1610395, 1610398), and Precision Protein StrepTactin-HRP Conjugate (Bio-Rad Laboratories, 1610381). Equal loading and quality of transfer was confirmed by staining membranes with Ponceau S (BioShop, PON002).

Immunofluorescent Analysis of MYH, and Determination of Cell Differentiation and Cell Fusion Index

For ad-BNIP3 experiments, cells were grown on glass coverslips coated with Cultrex basement membrane extract (Trevigen, 3432–010-01) placed in cell culture plates, whereas cells for ad-PRKN experiments were directly grown on cell culture plates. Coverslips and plates were removed at the appropriate timepoints (D3, D5) and were washed in PBS, fixed with fresh 4% formaldehyde-PBS for 5 min at room temperature, washed with PBS, permeabilized for 5 min with 0.5% Triton X-100, and further washed in PBS. Cells were then blocked with 10% goat serum-PBS (Cedarlane, CL1200) for 30 min, incubated with a primary antibody against MYH (Developmental

Studies Hybridoma Bank; MF20) diluted in blocking solution for 2 h, washed with PBS, and then incubated with an anti-mouse AlexaFluor488-conjugated secondary antibody (Invitrogen; A11001) for 1 h. Cells were washed in PBS, counterstained with 4′,6-diamidino-2-phenylindole (DAPI) nuclear stain (ThermoFisher Scientific, D3571) for 5 min, and washed in PBS. Ad-BNIP3 cells grown on coverslips were mounted with ProLong™ Glass Antifade Mountant (ThermoFisher Scientific, P36984) and microscope slides were visualized with an Axio Observer Z1 fluorescent microscope, equipped with standard Red/Blue/Green filters, an AxioCam HRm camera, and ZEN software (Carl Zeiss). Furthermore, ad-PRKN cells grown directly on cell culture plates were washed in PBS and visualized with a Cytation 5 cell imaging reader equipped with filter-based fluorescence detection and Gen5 software (BioTek).

As previously described [11], the differentiation index was calculated as the percentage of cells expressing MYH relative to the total number of cells. The cell fusion index was calculated as the percentage of nuclei present in multinucleated (two or more nuclei) cells relative to total nuclei.

Fluorescent Microscopy and Mitochondrial Network Branch and Puncta Analyses

As previously conducted in our lab [96], carbonyl cyanide 3-chlorophenylhydrazone (CCCP; Sigma-Aldrich C2759) concomitantly increased mitophagy and lipidation of MAP1LC3B. Transfected subconfluent cells with the pDsRed2-Mito vector were grown on glass coverslips and the following day (D0), cells were administered either GM supplemented with mdivi-1 (20 μM) or CCCP (50 μM) and incubated for 30 min at 37°C and 5% CO_2. For these experiments, vehicle control cells

were given GM with the equivalent chemical dilution of dimethyl sulfoxide (Veh; DMSO). Cells were washed in PBS, fixed with fresh 4% formaldehyde-PBS for 5 min at room temperature, and washed with PBS. After, cells were counterstained with DAPI, washed with PBS, mounted onto microscope slides using ProLong™ Glass Antifade Mountant, and imaged with an Axio Observer Z1 fluorescent microscope, equipped with Zeiss LSM 800 laser and ZEN software (Carl Zeiss).

As previously described [104], the mitochondrial network images were processed using Image J (National Institutes of Health) and validated built-in plugins quantified the mitochondrial network branch lengths, number of puncta, and the mitochondrial footprint as parameters for characterizing the mitochondrial network integrity. Briefly, the images were converted to a skeletonized map tracing the mitochondrial network. To quantify the morphological features of circularity and roundness, images were converted to 8-bit images and analyzed with the tubeness plugin. The mean number of junctions, branches, puncta, circularity, and roundness were tabulated from at least 10 or 25 different cells per group.

Statistics

A one-way ANOVA assessed the effect of differentiation within groups, with post-hoc analysis to determine differences from D0, except for CCCP differentiation experiments, which were compared to timepoint D1. Differences between time-matched Veh and mdivi-1 groups or Veh and CCCP groups were assessed using a Students T-test. For ad-DNM1L and ad-sh*Dnm1l* experiments, differences between time-matched ad-GFP control were assessed using multiple T-tests. A two-way ANOVA assessed

time-matched group differences in the transduced (ad-BNIP3, ad-PRKN) mdivi-1 differentiation experiments, with post-hoc analysis as appropriate. For all experiments $p < 0.05$ was considered statistically significant while $0.05 \leq p < 0.10$ was considered to approach statistical significance and we deemed this a statistical trend. All results shown are means ± standard error of the mean (SEM) and statistical analyses were performed with Graph Pad Prism Statistical Software.

4.0 Results

4.1 DNM1L inhibition impairs myoblast differentiation and myotube formation

We examined the effect of mitochondrial division inhibitor-1 (mdivi-1), a specific chemical inhibitor of DNM1L (dynamin 1-like protein) GTPase activity, on the process of mitochondrial fission during myoblast differentiation. Similar to our previous work [17], DNM1L levels upregulated in vehicle control cells (VEH) and decreased ($p < 0.05$) in the presence of 20 µM mdivi-1 (**Figure 1a,b**). Here, we reported that mitochondrial fusion protein MFN2 (mitofusin 2) remained elevated ($p < 0.05$) for both VEH and mdivi-1 treated cells upon the induction of differentiation (**Figure 1a,c**). Moreover, MYOG (myogenin) increased early in the differentiation program ($p < 0.05$) for both groups, but levels were significantly lower ($p < 0.05$) in mdivi-1 treated cells compared to VEH (**Figure 1a,d**). Further supporting the notion that mdivi-1 impaired myoblast differentiation, MYH (myosin heavy chain) dramatically decreased ($p < 0.05$) in mdivi-1 treated cells, with a concomitant decrease in the number of multinucleated MYH-positive myotubes (**Figure 1a,e-h**). Together, these data suggest that mdivi-1 decreased DNM1L function and disrupted myoblast differentiation.

4.2 DNM1L inhibition increases mitochondrial network branching, reduces autophagy, and increases mitochondrial apoptosis sensitivity

To further validate that mdivi-1 inhibited DNM1L function, we transfected C2C12 myoblasts with a pDsRed2-Mito reporter and visualized the mitochondrial network morphology. Overall, 20 µM mdivi-1 increased ($p < 0.05$) the mean branch lengths of mitochondria and inversely decreased ($p < 0.05$) the frequency of mitochondrial puncta (**Figure 2a-c**). In agreement with a hyperfused mitochondrial network, mdivi-1 treated

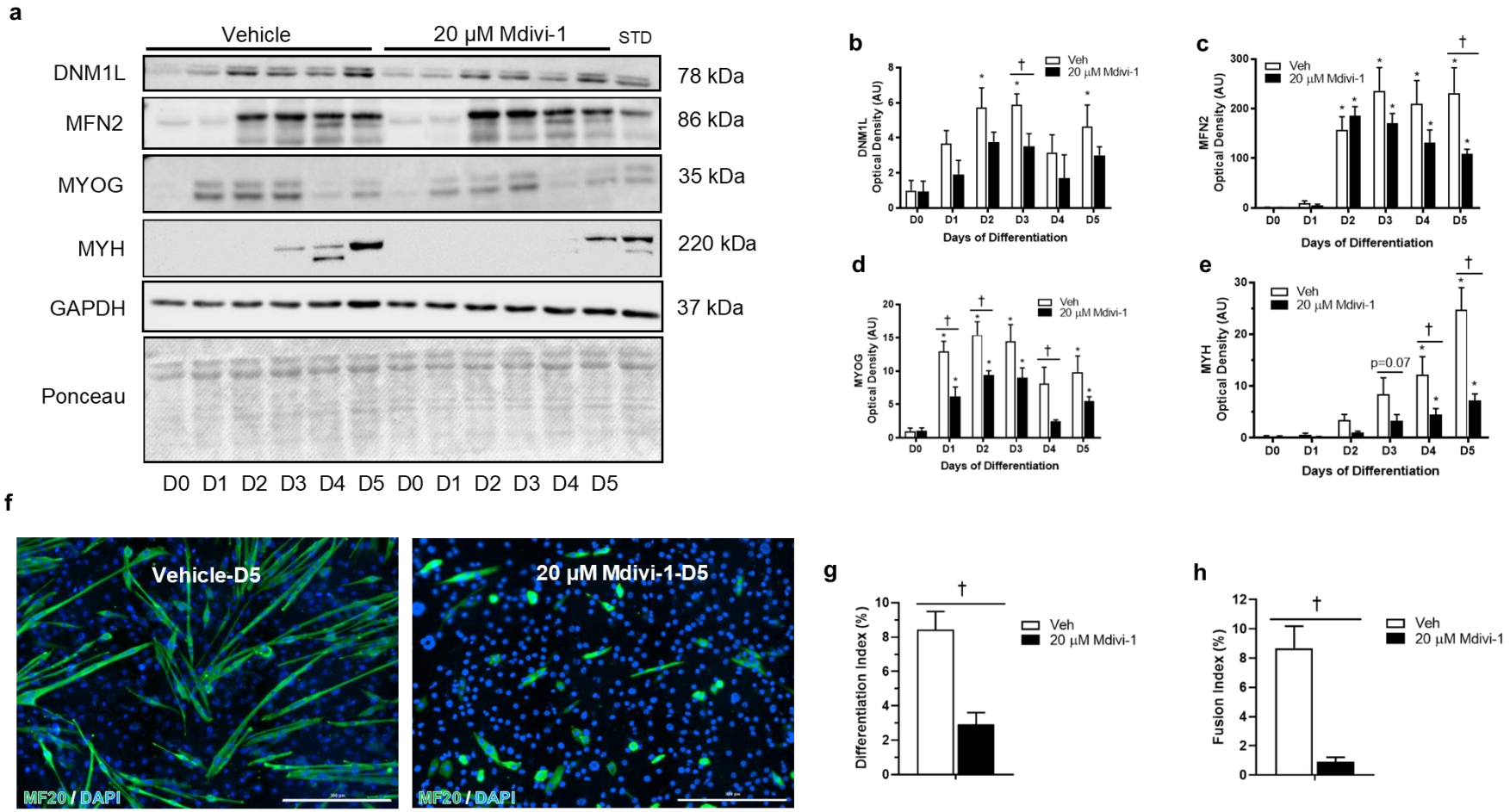

Figure 1. DNM1L inhibition with mdivi-1 disrupted C2C12 myogenic differentiation. Differentiated C2C12 cells were treated with vehicle (Veh) or 20 μM mdivi-1. Representative immunoblots (**a**) and quantitative analysis of mitochondrial fission protein DNM1L (**b**), mitochondrial fusion protein MFN2 (**c**), early and late differentiation markers MYOG (**d**) and MYH (**e**), respectively. Also shown are representative GAPDH and Ponceau loading control blots and a pooled sample standard (STD). Representative immunofluorescent images (**f**) of myotube formation in Veh and 20 μM mdivi-1 treated cells at Day 5 of differentiation. Cells were stained with DAPI (blue) and for MF20 (green) to visualize nuclei and MYH, respectively. Scale bar = 300 μm. Quantitative analysis of the differentiation index (**g**) and fusion index (**h**). *$p < 0.05$ compared to D0 (within group). †$p < 0.05$ between groups at the same timepoint.

cells exhibited a greater ($p < 0.05$) mean number of intersecting mitochondrial network junctions and approached statistical significance ($p < 0.10$) for triple and quadruple points compared to VEH (**Figure 2a,d-f**).

Autophagy proteins MAP1LC3B-I/LC3B-I (microtubule-associated protein 1 light chain 3 beta) and LC3B-II (lipidated form of MAP1LC3B-I) decreased in mdivi-1 treated cells ($p < 0.05$). Furthermore, the LC3B-II:I ratio decreased compared to VEH ($p < 0.05$, **Figure 2g-j**), which was accompanied by an initial SQSTM1 (sequestosome 1) accumulation, suggesting that autophagy was downregulated (**Figure 2g,k**).

A family of BCL2 (B cell leukemia/lymphoma 2)-related proteins are involved in the mitochondrial apoptosis pathway [105]. Despite no changes in the levels of pro-apoptotic BAX (BCL2-associated X, apoptosis regulator), we reported decreased ($p < 0.05$) anti-apoptotic BCL2 (BCL2 apoptosis regulator) levels with a tendency for elevated ($p < 0.10$) BAX:BCL2 ratio for mdivi-1 treated cells later on during differentiation (**Figure 2g,l-n**). In addition, DNA fragmentation marker p-H2AFX (phosphorylated H2A histone family, member X) transiently increased ($p < 0.05$) at D1 and VDAC1 (voltage-dependent anion channel 1) increased with no differences for mitochondrial content between groups (**Figure 2g,o,p**). Collectively, these findings suggest that mdivi-1 increased the sensitivity for BCL2 family-related apoptosis.

Figure 2. DNM1L inhibition with mdivi-1 increased mitochondrial network branching, decreased autophagy, and may increase intrinsic apoptosis sensitivity but not DNA fragmentation. Confocal microscope images (**a**) of C2C12 myoblasts transfected with pDsRed2-Mito (orange), treated with vehicle (Veh) or 20 µM mdivi-1 for 30 min at D0, then counterstained with nuclear dye DAPI (blue). n = 25 per group. Scale bar = 10 µm. Quantitative analysis of the summed mean mitochondrial branch length (**b**), calculated puncta (**c**; light blue), and mean number of junctions (**d**), triple points (**e**), and quadruple points (**f**). Representative immunoblots (**g**) and quantitative analysis of autophagosome machinery LC3B-I (**h**), LC3B-II (**i**), calculated LC3B-II:LC3B-I ratio (**j**), SQSTM1 (**k**), mitochondrial pro-apoptotic protein BAX (**l**) and anti-apoptotic protein BCL2 (**m**), calculated BAX:BCL2 ratio (**n**), DNA fragmentation marker p-H2AFX (**o**), and mitochondrial content marker VDAC1 (**p**). A GAPDH loading control blot is also shown. *$p < 0.05$ compared to D0 (within group). †$p < 0.05$ between groups at the same timepoint.

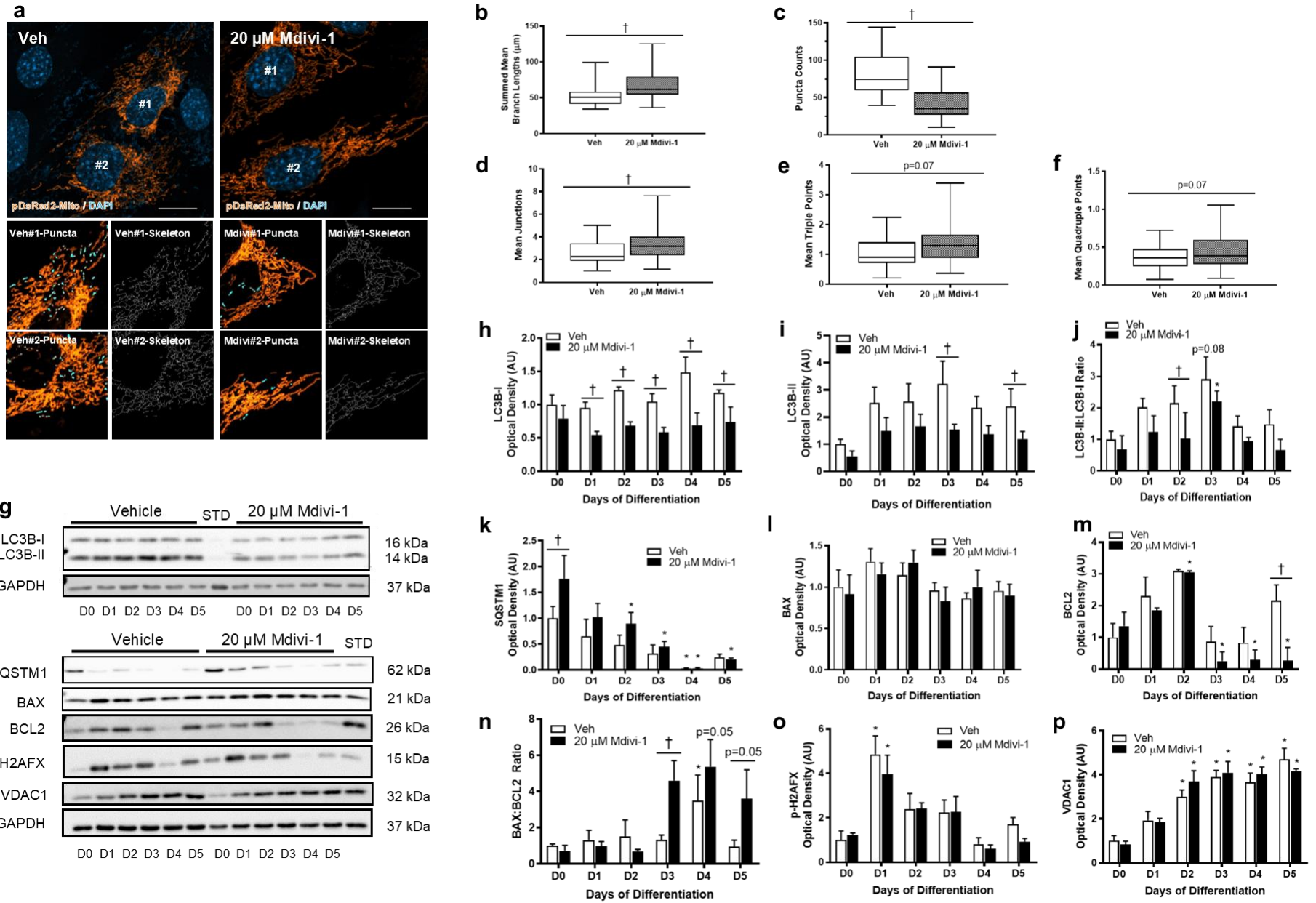
a
Veh
20 μM Mdivi-1
#1
#2
pDsRed2-Mito / DAPI
Veh#1-Puncta
Veh#1-Skeleton
Mdivi#1-Puncta
Mdivi#1-Skeleton
Veh#2-Puncta
Veh#2-Skeleton
Mdivi#2-Puncta
Mdivi#2-Skeleton
b
Summed Mean Branch Lengths (μm)
c
Puncta Counts
d
Mean Junctions
e
Mean Triple Points
p=0.07
f
Mean Quadruple Points
p=0.07
h
LC3B-I Optical Density (AU)
i
LC3B-II Optical Density (AU)
j
LC3B-II:LC3B-I Ratio
p=0.08
Veh
20 μM Mdivi-1
Days of Differentiation
g
Vehicle
STD
20 μM Mdivi-1
LC3B-I
LC3B-II
16 kDa
14 kDa
GAPDH
37 kDa
D0 D1 D2 D3 D4 D5
SQSTM1
62 kDa
BAX
21 kDa
BCL2
26 kDa
p-H2AFX
15 kDa
VDAC1
32 kDa
k
SQSTM1 Optical Density (AU)
l
BAX Optical Density (AU)
m
BCL2 Optical Density (AU)
n
BAX:BCL2 Ratio
p=0.05
p=0.05
o
p-H2AFX Optical Density (AU)
p
VDAC1 Optical Density (AU)

4.3 Inducing mitochondrial depolarization with CCCP promotes mitochondrial fission and stimulates LC3B-II conversion in autophagy

Since mdivi-1 increased mitochondrial network interconnectivity, we tested a potential chemical inducer of mitochondrial fission, carbonyl cyanide 3-chlorophenyl-hydrazone (CCCP). Cells transfected with a mitochondrial reporter and treated with 50 µM CCCP exhibited a decrease ($p < 0.05$) mitochondrial footprint that consisted of less mitochondrial branches per network and fewer total branches compared to VEH (**Figure 3a-c**). In support of this altered mitochondrial network morphology, the number of observed mitochondrial puncta increased ($p < 0.05$) suggesting that mitochondrial fission augmented (**Figure 3a,d**). Interestingly, the morphology of a subpopulation of mitochondria that were larger than puncta appeared circular and rounded ($p < 0.05$, **Figure 3a,e**). In agreement with this, the mean number of junctions and triple points decreased ($p < 0.05$), but no differences were observed for the mean number of quadruple points (**Figure 3a,f**). Collectively, these observations support that CCCP induced mitochondrial fission, but it is unclear whether DNM1L participated in the formation of these circular mitochondria.

Figure 3. Depolarization of mitochondria with CCCP increased LC3B-II and abolished mitochondrial network interconnectivity. Confocal microscope images (**a**) of C2C12 cells transfected with pDsRed2-Mito (orange), treated with either a vehicle (Veh) or 50 µM CCCP for 30 min at D0, then counterstained with nuclear dye DAPI (blue). Scale bar = 10 µm; Inset scale bar = 1 µm. Quantitative analysis of the skeletonized mitochondrial footprint (**b**), branches per network and total branches (**c**), puncta counts (**d**, light blue solid fill in **a**), mitochondrial circularity and roundness (**e**, light blue outline), and mean junctions, triple points, and quadruple points (**f**). n = 10 per group. Representative immunoblots (**g**) of differentiated C2C12 cells treated with 30 µM CCCP for 0 to 6 h and quantitative analysis of LC3B-I (**h**), LC3B-II (**i**), and calculated LC3B-II:LC3B-I ratio (**j**). Representative immunoblots (**k**) of differentiated C2C12 cells treated with 2.5 µM CCCP and quantitative protein analysis of DNM1L (**l**), BNIP3 (**m**), LC3B-I (**n**), LC3B-II (**o**), LC3B-II:LC3B-I ratio (**p**), SQSTM1 (**q**), MYH (**r**), BAX (**s**), BCL2 (**t**), calculated BAX:BCL2 ratio (**u**), and p-H2AFX (**v**). $^{\&}p < 0.05$ compared to 0 h (within group), $^{*}p < 0.05$ compared to D1 (within group), $^{\dagger}p < 0.05$ between groups at the same timepoint.

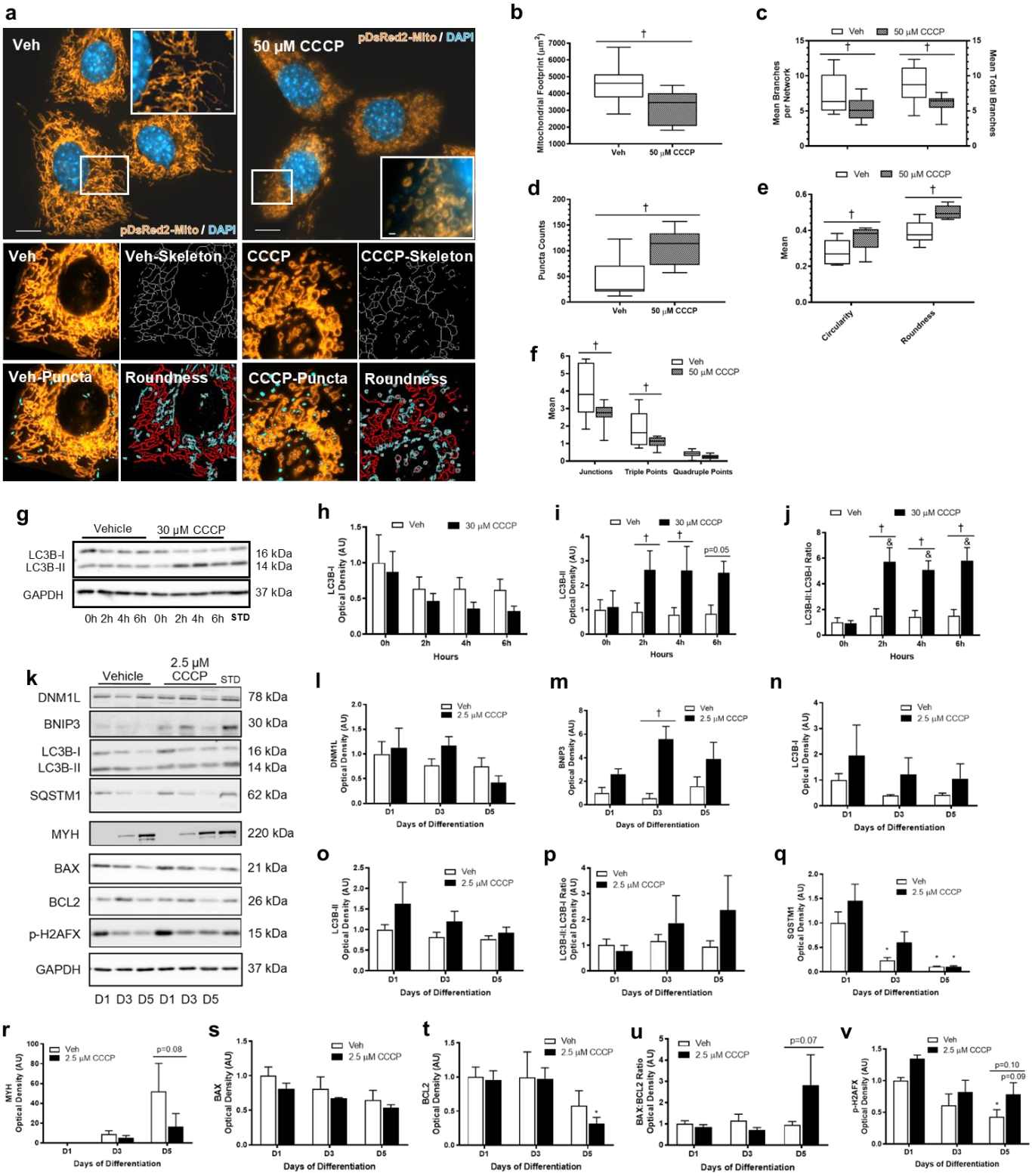
a
Veh
50 μM CCCP
pDsRed2-Mito / DAPI
Veh
Veh-Skeleton
CCCP
CCCP-Skeleton
Veh-Puncta
Roundness
CCCP-Puncta
Roundness
b
Mitochondrial Footprint (μm²)
Veh
50 μM CCCP
c
Veh
50 μM CCCP
Mean Branches per Network
Mean Total Branches
d
Puncta Counts
e
Mean
Circularity
Roundness
f
Mean
Junctions
Triple Points
Quadruple Points
g
Vehicle
30 μM CCCP
LC3B-I
LC3B-II
GAPDH
16 kDa
14 kDa
37 kDa
0h 2h 4h 6h 0h 2h 4h 6h STD
h
LC3B-I Optical Density (AU)
Hours
i
LC3B-II Optical Density (AU)
p=0.05
j
LC3B-II:LC3B-I Ratio
k
Vehicle
2.5 μM CCCP
STD
DNM1L
BNIP3
LC3B-I
LC3B-II
SQSTM1
MYH
BAX
BCL2
p-H2AFX
GAPDH
78 kDa
30 kDa
16 kDa
14 kDa
62 kDa
220 kDa
21 kDa
26 kDa
15 kDa
37 kDa
D1 D3 D5 D1 D3 D5
l
DNM1L Optical Density (AU)
Days of Differentiation
m
BNIP3 Optical Density (AU)
n
LC3B-I Optical Density (AU)
o
LC3B-II Optical Density (AU)
p
LC3B-II:LC3B-I Ratio Optical Density (AU)
q
SQSTM1 Optical Density (AU)
r
MYH Optical Density (AU)
p=0.08
s
BAX Optical Density (AU)
t
BCL2 Optical Density (AU)
u
BAX:BCL2 Ratio Optical Density (AU)
p=0.07
v
p-H2AFX Optical Density (AU)
p=0.10
p=0.09

Next, we examined the effect of CCCP on differentiated myoblasts. In the first 6 h of differentiation, LC3B-I levels were unaltered, but LC3B-II levels increased ($p < 0.05$) along with the LC3B-II:I ratio ($p < 0.05$, **Figure 3g-j**), suggesting that CCCP treatment stimulated autophagy. We then collected CCCP treated cells at later timepoints of differentiation but despite no differences in DNM1L content, mitophagy receptor BNIP3 (BCL2 interacting protein 3) levels increased compared to VEH ($p < 0.05$, **Figure 3k-m**). While there were no differences for LC3B-I levels, LC3B-II, and calculated LC3B-II:I ratio (**Figure 3k,n-p**), SQSTM1 levels decreased in CCCP treated cells ($p < 0.05$, **Figure 3k,q**), which had moderately lower levels of MYH ($p < 0.10$, **Figure 3k,r**). Despite BAX and BCL2 levels, as well as the BAX:BCL2 ratio remained unchanged ($p > 0.05$, **Figure 3k,s-u**), p-H2AFX levels were highest at D1 ($p < 0.10$, **Figure 3k,v**). Overall, we demonstrated that depolarization of mitochondria increased mitochondrial fission events, promoted autophagy, and in this context, yielded minor disruptions in the process of myoblast differentiation.

4.4 DNM1L overexpression increases BNIP3 levels during myoblast differentiation

To validate that DNM1L overexpression (ad-DNM1L) augmented DNM1L levels, we demonstrated that undifferentiated cells increased DNM1L content in a dose-dependent manner (**Supplementary Figure 1b**). Next, ad-DNM1L myoblasts were differentiated to investigate the effect of DNM1L overexpression during myoblast differentiation. DNM1L content increased stepwise ($p < 0.05$) at D3 and D5 (**Figure 4a,b**), with no differences between ad-DNM1L and ad-GFP control for FIS1 (fission, mitochondrial 1) and MFN2 levels (**Figure 4a,c,d**).

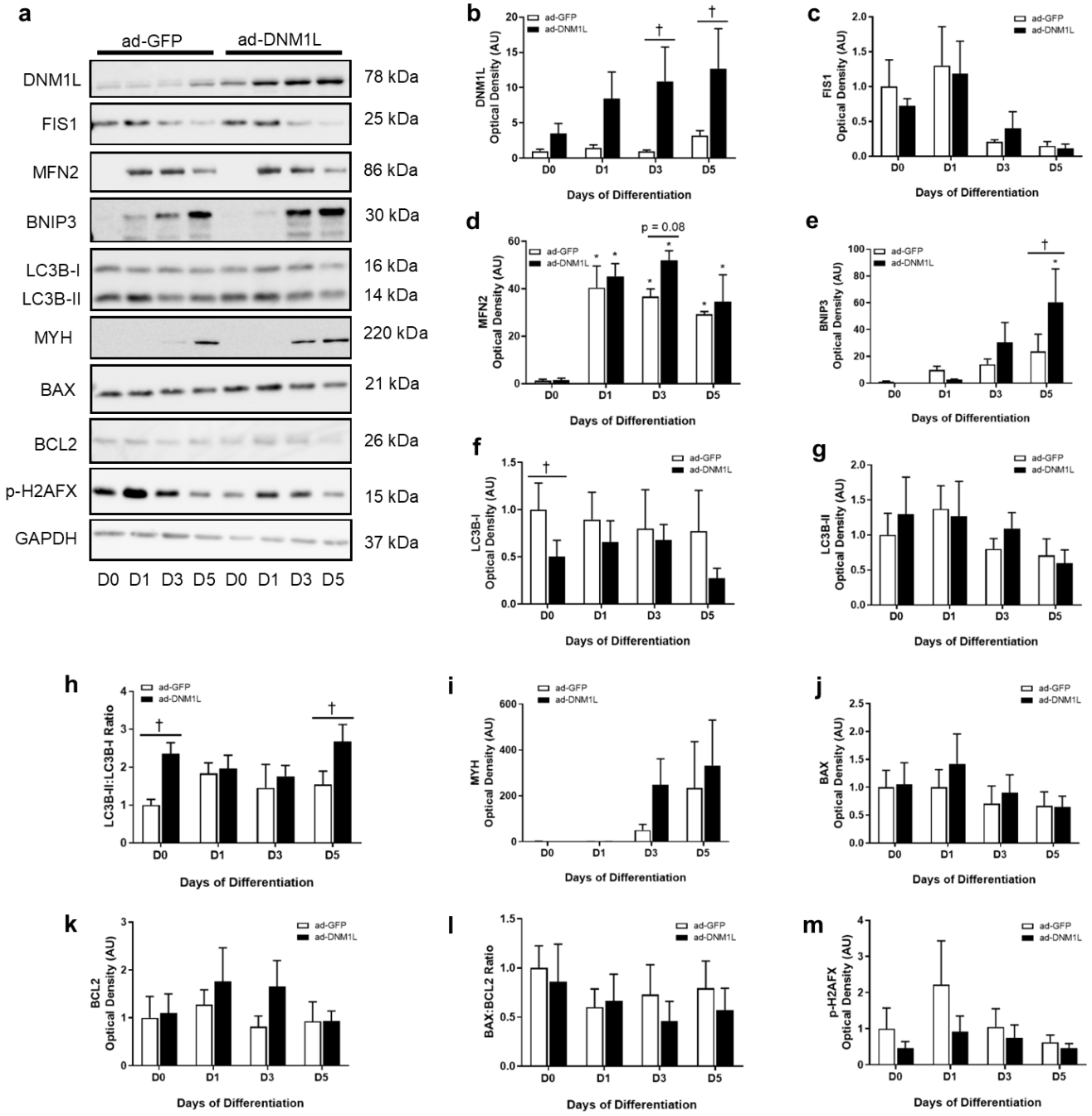

Figure 4. DNM1L overexpression maintained MYH protein levels and increased BNIP3 levels at D5. Representative immunoblots (**a**) of differentiated C2C12 cells transduced with ad-DNM1L. Quantitative analysis of mitochondrial network remodelling proteins DNM1L (**b**), FIS1 (**c**), MFN2 (**d**), mitophagy receptor BNIP3 (**e**), LC3B-I (**f**), LC3B-II (**g**), calculated LC3B-II:LC3B-I ratio (**h**), differentiation marker MYH (**i**), pro-apoptotic protein BAX (**j**), anti-apoptotic protein BCL2 (**k**), calculated BAX:BCL2 ratio (**l**), and DNA fragmentation marker p-H2AFX (**m**). *$p < 0.05$ compared to D0 (within group), †$p < 0.05$ compared to time-matched ad-GFP control group.

Importantly, BNIP3 increased 2.5-fold ($p < 0.05$) for ad-DNM1L cells (**Figure 4a,e**), and LC3B-I levels declined ($p < 0.05$) at D0 with no differences between LC3B-II levels, while the ratio of LC3B-II:I augmented compared to ad-GFP control (**Figure 4a,f-h**). Moreover, MYH levels were elevated at D5 relative to D0 (233-fold, ad-GFP control; 331-fold ad-DNM1L), but not statistically significant (**Figure 4a,i**). In agreement that DNM1L overexpression did not perturb myogenic differentiation, BAX and BCL2 levels, as well as the BAX:BCL2 ratio and p-H2AFX content indicated no differences ($p > 0.05$) between groups during differentiation (**Figure 4a,j-m**).

4.5 Genetic approach to reduce DNM1L expression and mitochondrial fission during myoblast differentiation

To provide further evidence that DNM1L is required for myoblast differentiation, we attempted to genetically knockdown DNM1L levels with a short hairpin RNA targeting *Dnm1l* (ad-sh*Dnm1l*, **Supplementary Figure 1c**). We found that DNM1L reduced by 65% ($p < 0.10$) at D5 for ad-sh*Dnm1l* compared to ad-GFP control while MFN2 levels remained unaffected (**Figure 5a-c**). Moreover, MYOG levels decreased ($p < 0.05$) compared to ad-GFP control (**Figure 5a,d**). In support of this, MYH levels were depressed ($p < 0.05$, **Figure 5a,e**) and SQSTM1 decreased by 83% at D5, but not statistically significant, relative to D0 (**Figure 5a,f**). BAX levels remained unchanged during differentiation (**Figure 5a,g**) and differences compared to ad-GFP control for p-H2AFX approached statistical significance at D1 ($p < 0.10$, **Figure 5a,h**). Together, these data possibly indicate that short hairpin RNA against *Dnm1l* may have disrupted myoblast differentiation in this context. However, a true knockdown experiment confirming that sh*Dnm1l* indeed decreases DNM1L warrants further investigation.

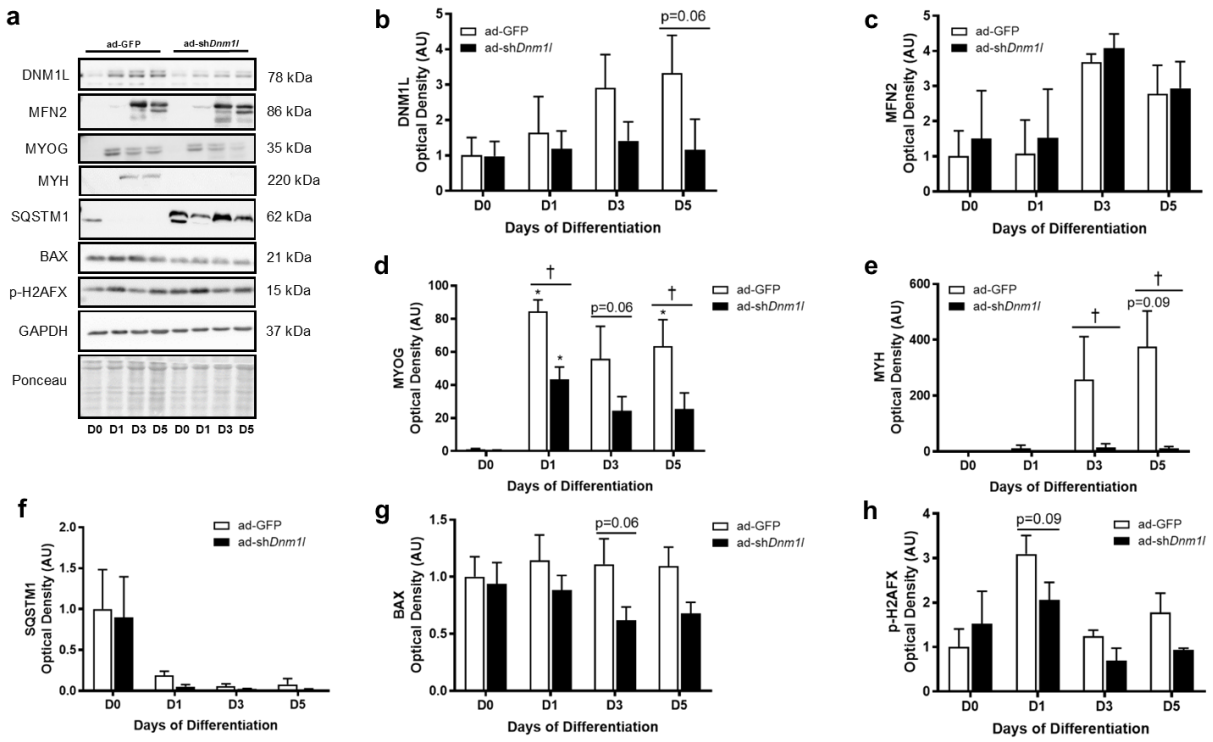

Figure 5. Short hairpin RNA against *Dnm1l* in differentiated myoblasts decreased MYOG and MYH levels. Representative immunoblots (**a**) and quantitative analysis of mitochondrial fission protein DNM1L (**b**), fusion protein MFN2 (**c**), early and late differentiation proteins MYOG (**d**) and MYH (**e**), respectively, autophagy-related protein SQSTM1 (**f**), and apoptosis proteins BAX (**g**) and p-H2AFX (**h**). *$p < 0.05$ compared to D0 (within group), †$p < 0.05$ compared to time-matched ad-GFP control group.

4.6 DNM1L inhibition and BNIP3 overexpression during myoblast differentiation

To examine the effect of BNIP3 in mdivi-1 treated cells, we overexpressed the mitophagy receptor BNIP3 (ad-BNIP3) during differentiation. Previous work demonstrated that BNIP3 was vital for C2C12 differentiation [11]. Indeed, BNIP3 levels increased ($p < 0.05$) in ad-BNIP3+Mdivi-1 treated cells compared to time-matched ad-GFP+Veh control (**Figure 6a,b**). Interestingly, BNIP3L/NIX (BCL2 interacting protein 3-like) levels decreased for all groups ($p < 0.05$; **Supplementary Figure 2a,c**), while DNM1L levels increased 3.6-fold at D5 for ad-BNIP3 groups compared to ad-GFP+Veh control ($p < 0.05$, **Figure 6a,c**). As expected, SQSTM1 levels dramatically decreased ($p < 0.05$) for all groups after the induction of the differentiation process (**Figure 6a,d**).

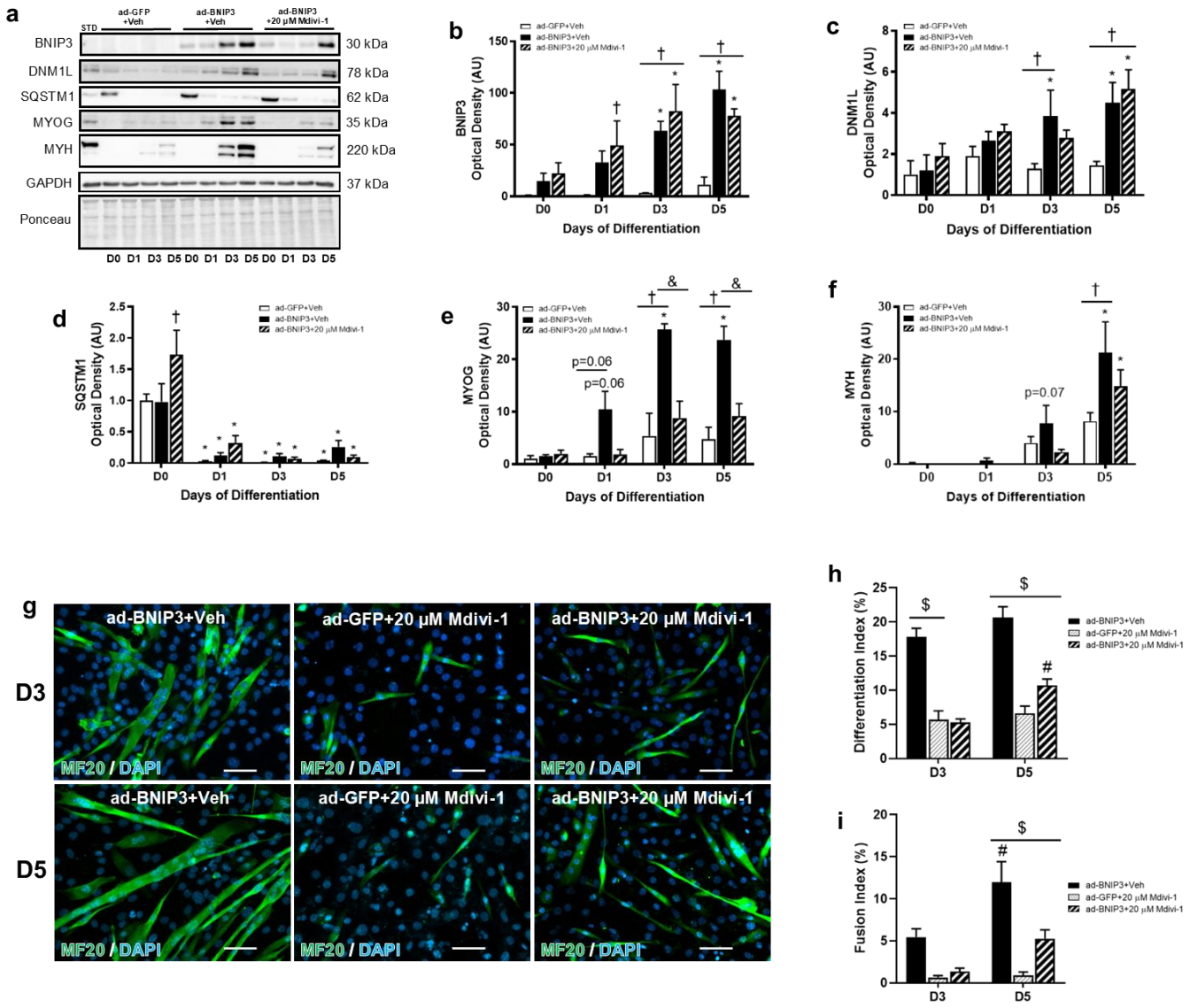

Figure 6. BNIP3 overexpression resulted in no impairments in myogenesis and BNIP3 overexpression in mdivi-1 treated myoblasts acutely restored myoblast cell fusion. Representative immunoblots (**a**) and quantitative analysis of mitophagy protein BNIP3 (**b**), mitochondrial fission protein DNM1L (**c**), autophagy-related protein SQSTM1 (**d**), early and late markers of differentiation MYOG (**e**) and MYH (**f**), respectively. Representative confocal microscopy images (**g**) of myotube formation in mdivi-1 treated cells at day 3 and day 5 of differentiation. Cells were stained with DAPI (blue) and for MF20 (green) to visualize nuclei and MYH, respectively. Scale bar = 100 μm. Quantitative analysis of the differentiation index (**h**) and fusion index (**i**). *$p < 0.05$ compared to D0 (within group), $^{\dagger}p < 0.05$ compared to time-matched ad-GFP+Veh group, $^{\&}p < 0.05$ compared to time-matched ad-BNIP3+Veh group, $^{\#}p < 0.05$ compared to D3 (within group), $^{\$}p < 0.05$ compared to time-matched ad-GFP+20 μM Mdivi-1 group.

Further supporting that BNIP3 overexpression did not impair myogenic differentiation, MYOG levels increased 5.0-fold ($p < 0.05$) for ad-BNIP3+Veh cells and mdivi-1 treatment exhibited no differences compared to ad-GFP+Veh control (**Figure 6a,e**). In alignment with these findings, MYH content increased ($p < 0.05$) at D5 for cells overexpressed with BNIP3 (**Figure 6a,f**). As further confirmation of the effect of BNIP3 overexpression in mdivi-1 treated cells, morphological analyses at D5 demonstrated increased ($p < 0.05$) MYH-positive cells and increased ($p < 0.05$) myoblast cell fusion compared to ad-GFP+Mdivi-1 cells (**Figure 6g-i**). These findings confirmed again that mdivi-1 impaired myotube formation and that BNIP3 overexpression in DNM1L inhibited cells partially recovered myoblast cell fusion during differentiation.

4.7 DNM1L shRNA and BNIP3 overexpression during myoblast differentiation

We then overexpressed BNIP3 in differentiated myoblasts transduced with ad-sh*Dnm1l* to examine whether BNIP3 compensated for DNM1L knockdown. Wistfully, we did not observe a knockdown effect as measured by DNM1L protein levels (**Figure 7a,b**). Nevertheless, we detected increased ($p < 0.10$) BNIP3 levels compared to ad-GFP control (**Figure 7a,c**). Interestingly, co-expression of ad-sh*Dnm1l* and ad-BNIP3 approached statistical significance ($p < 0.10$) for greater SQSTM1 levels at D0 compared to ad-GFP control, and decreased as expected by D5 relative to the induction of the differentiation process (**Figure 7a,d**).

Importantly, co-expression of ad-sh*Dnm1l* and ad-BNIP3 increased MYOG levels ($p < 0.05$, **Figure 7a,e**), which was accompanied by greater ($p < 0.05$) MYH levels in BNIP3 overexpressed cells compared to ad-GFP control (**Figure 7a,f**). While BAX

levels increased at D1 ($p < 0.05$), p-H2AFX levels were initially lower ($p < 0.05$) compared to ad-GFP control (**Figure 7a,g,h**). Collectively, these results could suggest that BNIP3 overexpression partially recovered the DNM1L-deficiency in myoblast differentiation. However, the effect of DNM1L knockdown utilizing the short hairpin RNA approach targeting *Dnm1l* requires further examination.

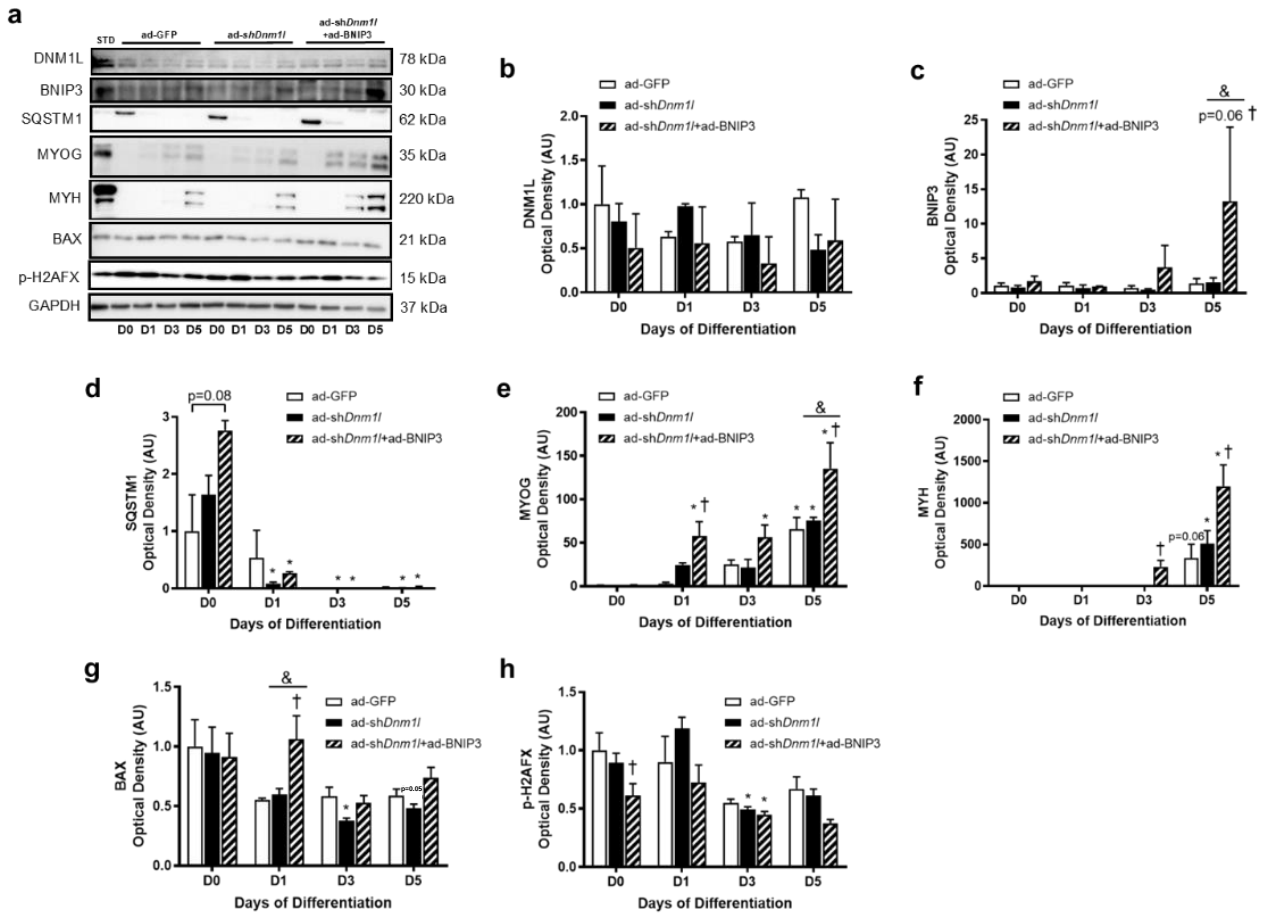

Figure 7. BNIP3 overexpression in differentiated sh*Dnm1l* myoblasts increased MYOG and MYH levels at D5. Representative immunoblots (**a**) and quantitative analysis of mitochondrial fission protein DNM1L (**b**), mitophagy protein BNIP3 (**c**) autophagy-related protein SQSTM1 (**d**), early and late markers of differentiation MYOG (**e**) and MYH (**f**), respectively, pro-apoptosis protein BAX (**g**), and DNA damage marker p-H2AFX (**h**). *$p < 0.05$ compared to D0 (within group), †$p < 0.05$ compared to time-matched ad-GFP group, &$p < 0.05$ compared to time-matched ad-sh*Dnm1l* group.

4.8 DNM1L mdivi-1 inhibition and PRKN overexpression during myoblast differentiation

Previous work conducted in our lab [96] demonstrated that C2C12 myoblasts lacked PRKN (parkin RBR E3 ubiquitin protein ligase). Indeed, we confirmed again in undifferentiated and differentiated cells (**Supplementary Figure 1e**) that C2C12 myoblasts were absent of PRKN. Interestingly, the PRKN-associated mitophagy receptor PINK1 (PTEN induced kinase 1) dramatically upregulated in ad-GFP+Veh control (**Figure 8a,b**). Thus, C2C12 myoblasts could present itself as a model for cells with PRKN-deficiency. To investigate the effect of PRKN on DNM1L inhibited cells, we overexpressed PRKN (ad-PRKN) in differentiated C2C12 myoblasts treated with mdivi-1. We reported that PRKN content increased ($p < 0.05$) for ad-PRKN+Mdivi-1 treated cells compared to ad-GFP+Veh control (**Figure 8a,c**), which also exhibited lower BNIP3 levels ($p < 0.05$, **Figure 8a,d**). While DNM1L content remained unaltered throughout differentiation (**Figure 8a,e**), SQSTM1 levels dramatically decreased ($p < 0.05$) for all groups suggesting that protein degradation upregulated after the induction of differentiation (**Figure 8a,f**). This was further supported by decreased LC3B-I levels ($p < 0.05$, **Figure 8a,g**) and increased LC3B-II levels ($p < 0.05$, **Figure 8a,h**) at D1 for ad-GFP-Veh control. However, LC3B-II levels for ad-PRKN+Mdivi-1 cells were lower ($p < 0.05$) but had an increased LC3B-II:I ratio at D5 ($p < 0.05$, **Figure 8a,i**).

Importantly, mdivi-1 treated cells overexpressed with PRKN had reduced MYOG levels ($p < 0.05$, **Figure 8a,j**) compared to ad-GFP+Veh control, suggesting that myoblast differentiation was impaired. In support of this, MYH content was supressed ($p < 0.05$, **Figure 8a,k**) in both ad-GFP+Mdivi-1 and ad-PRKN+Mdivi-1 groups

compared to ad-GFP+Veh control cells (**Supplementary Figure 3a,k**). In addition, immunofluorescent analyses for MYH-positive cells suggested that ad-PRKN+Veh treatment did not impair myotube formation (**Supplementary Figure 3m**). While p-H2AFX levels decreased ($p < 0.05$, **Figure 8a,l**) later during differentiation, DNM1L inhibited groups with and without PRKN overexpression exhibited a decreased ($p < 0.05$) differentiation response compared to ad-GFP+Veh control, as further demonstrated by the decreased proportion of MYH-positive cells (**Figure 8m,n**) and the corresponding lack of myoblast cell fusion ($p < 0.05$, **Figure 8m,o**). Collectively, these findings suggest that PRKN overexpression failed to ameliorate DNM1L inhibition by mdivi-1 during C2C12 myoblast differentiation.

Supplementary data related to this thesis can be found in the **Appendix**.

Figure 8. PRKN overexpression resulted in no impairments in myogenesis and PRKN overexpression in differentiated mdivi-1 treated myoblasts neither restored the protein levels of MYOG and MYH, nor increased the cell fusion of myoblasts. Representative immunoblots (**a**) and quantitative analysis of mitophagy proteins PINK1 (**b**), PRKN (**c**), and BNIP3 (**d**), mitochondrial fission protein DNM1L (**e**), autophagy-related protein SQSTM1 (**f**), LC3B-I (**g**), LC3B-II (**h**), and calculated LC3B-II:I ratio (**i**), early and late markers of differentiation MYOG (**j**) and MYH (**k**), respectively, and DNA damage marker p-H2AFX (**l**). Representative immunofluorescent images (**m**) of myotube formation in mdivi-1 treated cells at day 3 and day 5 of differentiation. Cells were stained with DAPI (blue) and for MF20 (green) to visualize nuclei and MYH, respectively. Scale bar = 100 µm. Quantitative analysis of the differentiation index (**n**) and fusion index (**o**). *$p < 0.05$ compared to D0 (within group), $^{\dagger}p < 0.05$ compared to time-matched ad-GFP+Veh control group, $^{\&}p < 0.05$ compared to time-matched ad-PRKN+Veh group, #$p < 0.05$ compared to D3 (within group).

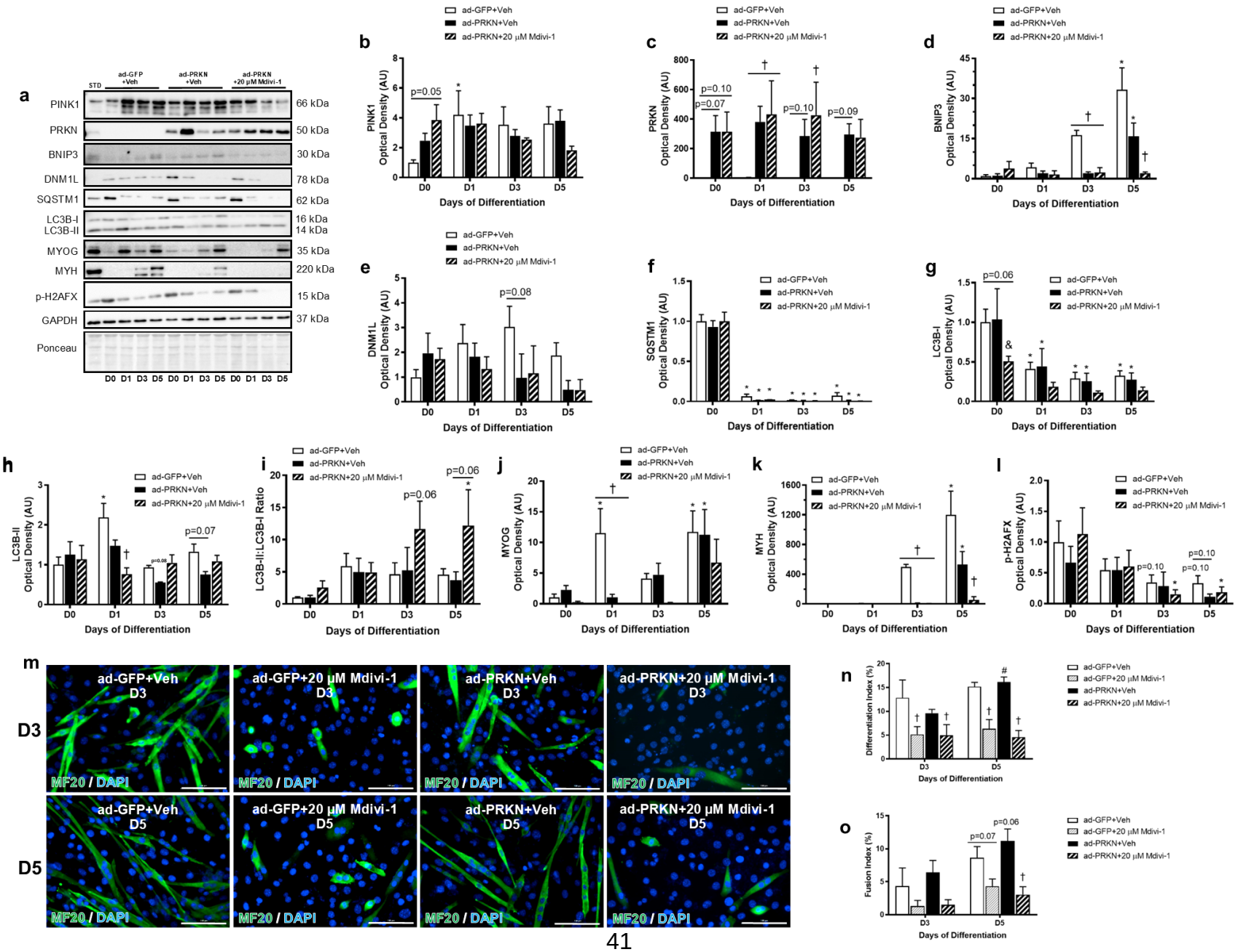
a
STD
ad-GFP +Veh
ad-PRKN +Veh
ad-PRKN +20 μM Mdivi-1
PINK1
PRKN
BNIP3
DNM1L
SQSTM1
LC3B-I
LC3B-II
MYOG
MYH
p-H2AFX
GAPDH
Ponceau
66 kDa
50 kDa
30 kDa
78 kDa
62 kDa
16 kDa
14 kDa
35 kDa
220 kDa
15 kDa
37 kDa
D0 D1 D3 D5 D0 D1 D3 D5 D0 D1 D3 D5
b
PINK1 Optical Density (AU)
p=0.05
c
PRKN Optical Density (AU)
p=0.10
p=0.07
p=0.10
p=0.09
d
BNIP3 Optical Density (AU)
e
DNM1L Optical Density (AU)
p=0.08
f
SQSTM1 Optical Density (AU)
g
LC3B-I Optical Density (AU)
p=0.06
h
LC3B-II Optical Density (AU)
p=0.07
i
LC3B-II:LC3B-I Ratio
p=0.06
p=0.06
j
MYOG Optical Density (AU)
k
MYH Optical Density (AU)
l
p-H2AFX Optical Density (AU)
p=0.10
p=0.10
p=0.10
ad-GFP+Veh
ad-PRKN+Veh
ad-PRKN+20 μM Mdivi-1
Days of Differentiation
D0
D1
D3
D5
m
D3
D5
ad-GFP+Veh D3
ad-GFP+20 μM Mdivi-1 D3
ad-PRKN+Veh D3
ad-PRKN+20 μM Mdivi-1 D3
ad-GFP+Veh D5
ad-GFP+20 μM Mdivi-1 D5
ad-PRKN+Veh D5
ad-PRKN+20 μM Mdivi-1 D5
MF20 / DAPI
n
Differentiation Index (%)
o
Fusion Index (%)
p=0.07
p=0.06

5.0 Discussion

5.1 DNM1L-dependent mitochondrial fission is inhibited by mdivi-1

The self-assembly of DNM1L is required for the scission of mitochondrial membranes and DNM1L oligomerization cooperatively promotes GTP hydrolysis [93], [106]. In a chemical screen for inhibitors of mitochondrial fission, Cassidy-Stone *et al*. [97] identified mitochondrial division inhibitor-1 (mdivi-1) as an allosteric inhibitor of GTP hydrolysis that blocked DNM1L oligomerization. Kinetic assay of the monomeric GTPase domain of $DNM1L^{1-338}$ and dynamin1-mediated endocytosis of clathrin-coated pits were unaffected by mdivi-1, suggesting that mdivi-1 was a selective inhibitor of DNM1L self-assembly which decreased DNM1L-dependent mitochondrial fission [98].

We examined an *in vitro* model for skeletal muscle differentiation with C2C12 myoblasts to determine the mitochondrial network morphology of myoblasts when treated with mdivi-1. Our study demonstrated that mdivi-1 treated C2C12 myoblasts exhibited decreased mitochondrial fission as evidenced by a hyperfused mitochondrial network which consisted of increased mitochondrial branching and reduced number of mitochondrial puncta. This was consistent with previous mitochondrial network analyses and strengthens the fact that mdivi-1 reduced mitochondrial fission [7], [17].

5.2 DNM1L-dependent mitochondrial fission, autophagy, and apoptosis during myoblast differentiation

Autophagy is required for myoblast differentiation [13], [15]. It was previously demonstrated that DNM1L-dependent mitochondrial fission accompanied the activation of autophagy in differentiated myoblasts [2]. In agreement with this, we reported that differentiated C2C12 control cells increased DNM1L content which coincided with the upregulation of autophagy. In contrast, differentiated myoblasts treated with mdivi-1

displayed reduced DNM1L levels and decreased autophagy as indicated by reduced LC3B-I to LC3B-II conversion. Furthermore, myoblasts treated with mdivi-1 initially showed SQSTM1 accumulation which supports that autophagy decreased in DNM1L inhibited cells. Thus, our findings indicated that reduced DNM1L-mediated mitochondrial fission with mdivi-1 corresponded to the reduction of autophagy during myoblast differentiation.

Myoblasts upregulate the expression of myogenic differentiation proteins MYOG and MYH, with MYOG appearing early in the differentiation process followed by MYH afterwards [91]. Here, we demonstrated that mdivi-1 treatment in C2C12 myoblasts impaired myogenic differentiation in agreement with others [7], [17]. Both MYOG and MYH levels were supressed and morphological analyses confirmed that the differentiation response and subsequent myoblast cell fusion significantly decreased compared to control cells. Collectively, our results demonstrated that DNM1L inhibition with mdivi-1 downregulated mitochondrial fission and blunted myotube formation.

Previous work showed that BCL2 family members of the mitochondrial apoptosis pathway were expressed early on during myoblast differentiation [107]. Although mitochondrial apoptosis was not our primary focus, we reported that control cells increased BAX levels early in the differentiation process which was matched by BCL2 levels. The ratio of BAX:BCL2, a common measure for apoptotic sensitivity of mitochondria [107], increased later in differentiation and this was consistent with others [105], [107]. In our study we present new data that mdivi-1 treated cells exhibited a greater BAX:BCL2 ratio suggesting that decreased mitochondrial fission increased the sensitivity for mitochondrial apoptosis in this context. Together, DNM1L inhibition

established that DNM1L was required for mitochondrial fission and provided evidence for an alternative role for DNM1L in the cellular processes of autophagy and apoptosis [97].

5.3 Depolarization of mitochondria stimulates autophagy

Previously, carbonyl cyanide 3-chlorophenylhydrazone (CCCP) stimulated mitochondrial membrane depolarization [107] and CCCP treated myoblasts increased LC3B-II levels [108]. In agreement with these studies, CCCP induced autophagy as indicated by increased LC3B-II:I ratio. Morphological analyses of the mitochondrial network in CCCP treated cells demonstrated a decreased mitochondrial footprint, which coincided with decreased total number of network branches, a greater frequency of mitochondrial puncta, and reduced the number of network junctions.

Interestingly, a subpopulation of mitochondria in CCCP treated myoblasts exhibited an unusual spheroid-shaped morphology. This was an unexpected result which was not reported by Türkseven & Zorzano [108]. However in another study utilizing MEF (mouse embryonic fibroblasts) and HeLa cells treated with 10 µM CCCP, confocal fluorescence and transmission electron microscopy (TEM) imaging revealed the distinct ring-shaped mitochondria after 10 min of treatment [109]. It was later confirmed that the lumen of spheroid mitochondria were contact sites with the endoplasmic reticulum and other organelles [109].

Intriguingly, differentiated C2C12 myoblasts treated with CCCP had higher BNIP3 levels compared to VEH. The observed upregulation of BNIP3 could be potentiated by the effect of myogenic differentiation. Above all, CCCP treated myoblasts displayed some decline in MYH levels and this was corroborated by a study that utilized

a range of CCCP concentrations [12]. Despite an inadequate understanding for the physiological relevance of CCCP, our results supported that CCCP stimulated autophagy which could be a protective response to the detrimental effects of mitochondrial depolarization. CCCP deteriorated the mitochondrial network interconnectivity which may involve DNM1L as suggested by others [110], but another study suggested that the effect of CCCP was independent of DNM1L [109]. Nevertheless, the morphology of mitochondria was drastically altered in the presence of CCCP which establishes a basis for further studies examining the mechanisms of mitochondrial fission and fusion that favour the remodelling of network morphology.

5.4 Overexpression of DNM1L and short hairpin RNA against *Dnm1l* during myoblast differentiation

We examined the effect of DNM1L overexpression (ad-DNM1L) or knockdown (ad-sh*Dnm1l*) during myoblast differentiation. Interestingly, ad-DNM1L increased BNIP3 levels and concomitantly increased LC3B-II:I conversion, suggesting that DNM1L and BNIP3 are related in autophagy. This was further supported by fluorescence microscopy in cardiac myocytes overexpressing BNIP3 which had reduced LC3B-II levels when DNM1L was inhibited with mdivi-1, implying that DNM1L played an important role in BNIP3-induced autophagy [111]. Furthermore, we demonstrated that MYH levels were unaltered for ad-DNM1L cells compared to control.

While differentiated ad-sh*Dnm1l* cells trended towards statistical significance for DNM1L knockdown, myoblasts significantly exhibited reduced MYOG and MYH levels throughout differentiation. Granted that measurable differences of MYH levels were observed, the reduction of DNM1L as an inference of decreased mitochondrial fission events should be loosely interpreted in this context. An effective knockdown of DNM1L

would further confirm the effects of decreased mitochondrial fission on myoblast differentiation as we previously demonstrated by the action of mdivi-1. Together, overexpression of DNM1L appeared to preserve MYH levels whereas sh*Dnm1l* may have impaired myoblast differentiation suggesting that sh*Dnm1l* could have decreased DNM1L-dependent mitochondrial fission during myoblast differentiation.

5.5 DNM1L inhibition and BNIP3 overexpression during myoblast differentiation

Skeletal muscle development and repair requires the differentiation of activated myoblasts [91]. Myoblasts restructure their mitochondrial network and shift from a glycolytic metabolism to mitochondrial oxidative phosphorylation during myoblast differentiation [2]. Since myoblasts dramatically remodel the morphology of mitochondria, it is reasonable that mitochondrial fission permits the exclusion of a subpopulation of mitochondria and promotes the mitophagy of these mitochondria.

Previous work utilizing differentiated BNIP3-deficient C2C12 myoblasts (*bnip3*$^{-/-}$) showed decreased DNM1L levels and abolished MYOG and MYH [11]. Here we demonstrated the effect of BNIP3 overexpression (ad-BNIP3) in differentiated myoblasts inhibited with mdivi-1 which upregulated BNIP3 content and significantly increased MYOG and MYH levels. Ad-BNIP3 mdivi-1 treated myoblasts upregulated endogenous DNM1L levels and this further supports the idea that BNIP3 and DNM1L are involved in related pathways at the level of the mitochondria. In a similar way, hyper-fusion of mitochondria with a dominant-negative form of DNM1L (DNM1L^{K38E}) in cardiac myocytes suppressed endogenous BNIP3 levels [111]. As further confirmation that ad-BNIP3 partially rescued DNM1L inhibition in differentiated myoblasts, the proportion of MYH-positive cells increased, and the cell fusion of myoblasts ameliorated

for mdivi-1 treated myoblasts. Supplementing our findings of DNM1L inhibition, we attempted to co-express ad-sh*Dnm1l* and ad-BNIP3 in differentiated myoblasts. Although we did not achieve a knockdown of DNM1L, BNIP3 overexpression resulted in greater MYOG and MYH levels. Collectively, the new data reported here suggest that the mitophagy receptor BNIP3 promoted myotube formation in DNM1L inhibited myoblasts.

Given that (1) BNIP3-deficient myoblasts reduced endogenous DNM1L levels [11], and (2) BNIP3 overexpression partially recovered mdivi-1 DNM1L inhibition, and (3) overexpression of either BNIP3 or DNM1L increased the protein content of the other, we postulate that BNIP3 and DNM1L cooperatively remodel the mitochondrial network during myotube formation. Future studies investigating the overexpression of DNM1L in *bnip3*$^{-/-}$ myoblasts would elucidate the complementary effect of increased DNM1L-dependent mitochondrial fission in the context of BNIP3 deficiency during myoblast differentiation. Collectively, we demonstrated a novel effect for BNIP3 overexpression in DNM1L inhibited C2C12 myoblasts during myotube formation.

5.6 DNM1L inhibition and PRKN overexpression during myoblast differentiation

Emerging studies demonstrated that PINK1 stabilization on the outer mitochondrial membrane and the subsequent recruitment of PRKN promotes the degradation of select mitochondria [12], [60]. Considering that PRKN recruitment was noted during BNIP3-induced mitophagy in cardiac myocytes and mouse embryonic fibroblasts [88], [111], in our study we examined the role of PRKN in the context of DNM1L inhibition during C2C12 myoblast differentiation. Previous work in our lab [96] demonstrated that proliferating primary mouse, primary human, and immortalized L6 rat

cells expressed low PRKN levels, which upregulated during myogenic differentiation. However, proliferating C2C12 myoblasts, control myoblasts, and myoblasts treated with CCCP or starved with Hank's balanced salt solution (HBSS/amino acid withdrawal) did not express detectable levels of PRKN, including C2C12 myoblasts subjected to 5 days of differentiation. Furthermore, the lack of detectable PRKN levels was also documented by others in HeLa cells and this was exploited as a model for PRKN-independent mitophagy [60], [62], [112]. Thus, we utilized this unique characteristic of C2C12 myoblasts to examine the effect of PRKN overexpression in differentiated DNM1L inhibited myoblasts. In the absence of PRKN, C2C12 myoblasts could rely on BNIP3 as a key mitophagy receptor during C2C12 myoblast differentiation.

We confirmed again that PRKN was absent in both untransduced proliferating and differentiated C2C12 myoblasts. Upon the overexpression of PRKN (ad-PRKN), we detected through immunoblotting a PRKN protein product at the predicted molecular weight. We also detected PINK1 levels in control myoblasts which displayed no differences for PINK1 levels between ad-PRKN and control groups during differentiation. While PRKN overexpression in control cells still formed myotubes, interestingly ad-PRKN mdivi-1 treated myoblasts had significantly reduced MYOG and MYH levels, suggesting that PRKN overexpression exacerbated DNM1L inhibition during myotube formation. Further confirming that PRKN overexpression did not rescue mdivi-1 inhibition of DNM1L, we noted a reduction in the proportion of MYH-positive cells and fewer myoblast cell fusion events compared to ad-GFP control.

It is unclear how BNIP3 and PINK1 interact on the surface of mitochondria to recruit PRKN in differentiated C2C12 myoblasts when we present here that myoblasts

are absent of endogenous PRKN. Our results which indicated that myoblasts lacked detectable levels of PRKN are contradicted by a study that examined PRKN content in differentiated C2C12 myoblasts [12]. However, in the same study BNIP3 levels were not measured, further amplifying the need for studies investigating the interaction of BNIP3 and PINK1 on the possible recruitment of PRKN to the mitochondria in C2C12 myoblasts.

5.7 A dual function of BNIP3 in mitophagy and apoptosis

The mitophagy receptor BNIP3 contains a BH3-only domain that can interact with pro-apoptotic BAX and anti-apoptotic BCL2 proteins [20]. However, the mechanism of how BNIP3 induces cell death merits further research because BNIP3 can be exploited as a molecular switch between mitophagy and cell death [39], [68]. In our study, BNIP3 overexpression partly compensated for the mitochondrial fission deficiency achieved by mdivi-1 and permitted C2C12 myoblast differentiation. An advantage for BNIP3 mitochondrial localization is the potential role for inducing mitophagy as a repair mechanism to prevent premature cell death [20], [54]. It is possible that mdivi-1 treated cells overexpressed with BNIP3 had sufficient levels of BNIP3 present to interact with other BH3-only proteins such as BAX, BCL2, and BECN1, each with reported functions for promoting cell death, cell survival, and autophagy [39], [113], [114]. In contrast, PRKN is absent of a BH3-only domain and thus possibly lacks the same level of control as BNIP3 governing the signaling events in response to DNM1L inhibition during myoblast differentiation.

5.8 Limitations and future directions

Our study further demonstrated that DNM1L inhibition with mdivi-1 impaired C2C12 myoblast differentiation. With the new data reported here, we found that BNIP3 overexpression partially restored myoblast differentiation for DNM1L inhibited cells despite no effect with PRKN overexpression. However, some limitations can be addressed with follow-up studies. One example was the use of a mitochondrial fluorescent reporter because transfections induces stress to cells which can affect the morphology of the mitochondrial network. Thus, using more than one method to visualize mitochondria would support our mitochondrial network analyses. This can be achieved with photostable chemical dyes specific for mitochondrial staining (e.g. MitoTracker) [17], [115]. With respect to the mitochondrial puncta observed in CCCP treated cells, co-expression of a LC3 reporter then chloroquine treatment to block autophagosome-lysosome fusion, would identify mitochondria targeted for autophagy. Previously, the pDsRed2-Mito reporter was used in conjunction with a GFP-tagged LC3 expression vector to quantify colocalization events as a measure for mitophagy [11].

We attempted to genetically knockdown DNM1L with a short hairpin RNA against *Dnm1l* (sh*Dnm1l*). A shortcoming of our knockdown experiments was the effectiveness of the knockdown on reducing DNM1L levels. Despite the reduction of DNM1L content which approached statistical significance, future studies should validate the knockdown effect of sh*Dnm1l* with increased adenoviral multiplicity of infection (MOI), a measure of the ratio of viral particles to the number of host cells used to standardize cell culture transduction experiments.

It was established in the literature that DNM1L translocation to the mitochondria mediates mitochondrial fission [5], [74], [94]. In our study, we measured DNM1L content in whole cell lysates. Although we observed reductions in DNM1L content for both mdivi-1 treated and sh*Dnm1l* cells, the cellular localization of DNM1L would reinforce our findings. This can be accomplished by subcellular fractionation and centrifugation techniques that separate the cellular compartments of the nucleus, cytosol, and mitochondria-enriched fractions [11].

To study the interplay between DNM1L and mitophagy receptors, we treated C2C12 myoblasts with mdivi-1 then overexpressed BNIP3 or PRKN. As noted earlier, subcellular fractionation could advance our findings and further support the relationship between DNM1L and mitophagy proteins. Moreover, a future study utilizing CRISPR-Cas9 generated *bnip3*$^{-/-}$ myoblasts could examine whether DNM1L or PRKN overexpression recovers the abolished levels of MYH observed in differentiated BNIP3-deficient myoblasts [11].

Mitochondrial dynamics of fission and fusion as well as the biogenesis and degradation of mitochondria all contribute to the remodelling of the mitochondrial network [3], [23], [116]. Our study could further examine the levels of mitochondrial fusion and mitochondrial biogenesis proteins in the context of DNM1L inhibition during myoblast differentiation. In short, future studies investigating the effect of DNM1L inhibition or DNM1L knockdown on other mitochondrial network remodelling processes should be conducted.

5.9 Summary and Conclusion

In this study we showed that DNM1L inhibition decreased mitochondrial fission and impaired C2C12 myoblast differentiation. Through a combination of mitochondrial network analyses and MYH expression-based experiments, we demonstrated that mdivi-1 resulted in a hyperfused mitochondrial network while CCCP stimulated mitochondrial fission. Importantly, we identified that BNIP3 overexpression partially recovered myoblast cell fusion for DNM1L inhibited cells during myoblast differentiation. However, we found that PRKN overexpression in mdivi-1 treated myoblasts did not rescue myotube formation to the same extent. Thus, our findings further support the requirement for DNM1L and the involvement of mitophagy receptors during myoblast differentiation.

6.0 References

[1] A. C. Keefe *et al.*, “Muscle stem cells contribute to myofibres in sedentary adult mice,” *Nat. Commun.*, vol. 6, no. May, pp. 1–11, 2015, doi: 10.1038/ncomms8087.

[2] J. Sin *et al.*, “Mitophagy is required for mitochondrial biogenesis and myogenic differentiation of C2C12 myoblasts,” *Autophagy*, vol. 12, no. 2, pp. 369–380, 2016, doi: 10.1080/15548627.2015.1115172.

[3] A. Stotland and R. A. Gottlieb, “Mitochondrial quality control: Easy come, easy go,” *Biochim. Biophys. Acta - Mol. Cell Res.*, vol. 1853, no. 10, pp. 2802–2811, Oct. 2015, doi: 10.1016/j.bbamcr.2014.12.041.

[4] X. Liu, D. Weaver, O. Shirihai, and G. Hajnóczky, “Mitochondrial kiss-and-run: Interplay between mitochondrial motility and fusion-fission dynamics,” *EMBO J.*, vol. 28, no. 20, pp. 3074–3089, 2009, doi: 10.1038/emboj.2009.255.

[5] G. Twig *et al.*, “Fission and selective fusion govern mitochondrial segregation and elimination by autophagy,” *EMBO J.*, vol. 27, no. 2, pp. 433–446, 2008, doi: 10.1038/sj.emboj.7601963.

[6] L. Galluzzi, O. Kepp, and G. Kroemer, “Mitochondrial dynamics: A strategy for avoiding autophagy,” *Curr. Biol.*, vol. 21, no. 12, pp. R478–R480, 2011, doi: 10.1016/j.cub.2011.05.002.

[7] B. Kim, J.-S. Kim, Y. Yoon, M. C. Santiago, M. D. Brown, and J.-Y. J.-Y. Park, “Inhibition of Drp1-dependent mitochondrial division impairs myogenic differentiation,” *AJP Regul. Integr. Comp. Physiol.*, vol. 305, no. 8, pp. R927–R938, Oct. 2013, doi: 10.1152/ajpregu.00502.2012.

[8] G. Twig and O. S. Shirihai, “The Interplay Between Mitochondrial Dynamics and Mitophagy,” *Antioxid. Redox Signal.*, vol. 14, no. 10, pp. 1939–1951, 2011, doi: 10.1089/ars.2010.3779.

[9] G. Twig, B. Hyde, and O. S. Shirihai, “Mitochondrial fusion, fission and autophagy as a quality control axis: The bioenergetic view,” *Biochim. Biophys. Acta - Bioenerg.*, vol. 1777, no. 9, pp. 1092–1097, 2008, doi: 10.1016/j.bbabio.2008.05.001.

[10] T. Johansen and T. Lamark, “Selective autophagy mediated by autophagic adaptor proteins,” *Autophagy*, vol. 7, no. 3, pp. 279–296, 2011, doi: 10.4161/auto.7.3.14487.

[11] B. L. Baechler, D. Bloemberg, and J. Quadrilatero, “Mitophagy regulates mitochondrial network signaling , oxidative stress , and apoptosis during myoblast differentiation apoptosis during myoblast differentiation,” *Autophagy*, pp. 1–14, 2019, doi: 10.1080/15548627.2019.1591672.

[12] N. Peker, V. Donipadi, M. Sharma, C. McFarlane, and R. Kambadur, “Loss of Parkin impairs mitochondrial function and leads to muscle atrophy,” *Am J Physiol Cell Physiol*, no. 59, p. In press, 2018, doi: 10.1152/ajpcell.00064.2017.

[13] R. Chen *et al.*, “Effects of Cobalt Chloride, a Hypoxia-Mimetic Agent, on Autophagy and Atrophy in Skeletal C2C12 Myotubes,” *Biomed Res. Int.*, vol. 2017, pp. 1–9, 2017, doi: 10.1155/2017/7097580.

[14] W. X. Ding and X. M. Yin, “Mitophagy: Mechanisms, pathophysiological roles, and analysis,” *Biochem. J.*, vol. 393, no. 7, pp. 547–564, 2012, doi: 10.1515/hsz-2012-0119.

[15] E. M. McMillan and J. Quadrilatero, “Autophagy is required and protects against apoptosis during myoblast differentiation,” *Biochem. J.*, vol. 462, no. 2, pp. 267–277, 2014, doi: 10.1042/BJ20140312.

[16] C. Mammucari *et al.*, “FoxO3 Controls Autophagy in Skeletal Muscle In Vivo,” *Cell Metab.*, vol. 6, no. 6, pp. 458–471, 2007, doi: 10.1016/j.cmet.2007.11.001.

[17] D. Bloemberg and J. Quadrilatero, “Effect of mitochondrial fission inhibition on C2C12 differentiation,” *Data Br.*, vol. 7, pp. 634–640, 2016, doi: 10.1016/j.dib.2016.02.070.

[18] Z. Yang and D. J. Klionsky, “Eaten alive: A history of macroautophagy,” *Nat. Cell Biol.*, vol. 12, no. 9, pp. 814–822, 2010, doi: 10.1038/ncb0910-814.

[19] H. Nakatogawa, K. Suzuki, Y. Kamada, and Y. Ohsumi, “Dynamics and diversity in autotophagy mechanisms: lessons from yeast,” *Nature Reviews*, vol. 10, no. 7. pp. 458–467, 2009.

[20] T. R. Burton and S. B. Gibson, “The role of Bcl-2 family member BNIP3 in cell death and disease: NIPping at the heels of cell death,” *Cell Death Differ.*, vol. 16, no. 4, pp. 515–523, 2009, doi: 10.1038/cdd.2008.185.

[21] R. A. Hanna, M. N. Quinsay, A. M. Orogo, K. Giang, S. Rikka, and Å. B. Gustafsson, “Microtubule-associated protein 1 light chain 3 (LC3) interacts with Bnip3 protein to selectively remove endoplasmic reticulum and mitochondria via autophagy,” *J. Biol. Chem.*, vol. 287, no. 23, pp. 19094–19104, 2012, doi: 10.1074/jbc.M111.322933.

[22] C. He and D. J. Klionsky, “Regulation Mechanisms and Signaling Pathways of Autophagy,” *Annu. Rev. Genet.*, vol. 43, no. 1, pp. 67–93, 2009, doi: 10.1146/annurev-genet-102808-114910.

[23] V. Romanello and M. Sandri, “Mitochondrial quality control and muscle mass maintenance,” *Front. Physiol.*, vol. 6, no. JAN, pp. 1–21, 2016, doi: 10.3389/fphys.2015.00422.

[24] M. Laplante *et al.*, “mTOR signaling at a glance.,” *J. Cell Sci.*, vol. 122, no. Pt 20, pp. 3589–94, 2009, doi: 10.1242/jcs.051011.

[25] I. G. Ganley, D. H. Lam, J. Wang, X. Ding, S. Chen, and X. Jiang, “ULK1·ATG13·FIP200 complex mediates mTOR signaling and is essential for autophagy,” *J. Biol. Chem.*, vol. 284, no. 18, pp. 12297–12305, 2009, doi: 10.1074/jbc.M900573200.

[26] N. Hosokawa *et al.*, “Nutrient-dependent mTORC1 Association with the ULK1–Atg13–FIP200 Complex Required for Autophagy,” *Mol. Cell. Biol.*, vol. 20, pp.

1981–1991, 2009, doi: doi/10.1091/mbc.E08–12–1248.

[27] C. Hwa Jung *et al.*, “ULK-Atg13-FIP200 Complexes Mediate mTOR Signaling to the Autophagy Machinery,” *Mol. Cell. Biol.*, vol. 20, pp. 1992–2003, 2009, doi: 10.1091/mbc.E08-12-1249.

[28] J. Xu, M. Fotouhi, and P. S. Mcpherson, “Phosphorylation of the exchange factor DENND3 by ULK in response to starvation activates Rab12 and induces autophagy,” *EMBO Rep.*, vol. 16, no. 6, pp. 709–718, 2015, doi: 10.15252/embr.

[29] B. D. Manning, A. R. Tee, M. N. Logsdon, J. Blenis, and L. C. Cantley, “Identification of the Tuberous Sclerosis Complex-2 Tumor Suppressor Gene Product Tuberin as a Target of the Phosphoinositide 3- Kinase / Akt Pathway,” *Cell*, vol. 10, pp. 151–162, 2002, doi: 10.1016/S1097276502005683.

[30] B. Levine and G. Kroemer, “Autophagy in the Pathogenesis of Disease,” *Cell*, vol. 132, no. 1, pp. 27–42, 2008, doi: 10.1016/j.cell.2007.12.018.

[31] A. Hamacher-Brady *et al.*, “Response to myocardial ischemia/reperfusion injury involves Bnip3 and autophagy,” *Cell Death Differ.*, vol. 14, no. 1, pp. 146–157, 2007, doi: 10.1038/sj.cdd.4401936.

[32] K. Suzuki, T. Kirisako, Y. Kamada, N. Mizushima, T. Noda, and Y. Ohsumi, “The pre-autophagosomal structure organized by concerted functions of APG genes is essential for autophagosome formation,” *EMBO J.*, vol. 20, no. 21, pp. 5971–5981, 2001, doi: 10.1093/emboj/20.21.5971.

[33] K. Suzuki, Y. Kubota, T. Sekito, and Y. Ohsumi, “Hierarchy of Atg proteins in pre-autophagosomal structure organization,” *Genes to Cells*, vol. 12, no. 2, pp. 209–218, 2007, doi: 10.1111/j.1365-2443.2007.01050.x.

[34] Y. Tanaka *et al.*, “Accumulation of autophagic vacuoles and cardiomyopathy LAMP-2-deficient mice,” *Nature*, vol. 406, no. 6798, pp. 902–906, 2000, doi: 10.1038/35022595.

[35] S. Jager, “Role for Rab7 in maturation of late autophagic vacuoles,” *J. Cell Sci.*, vol. 117, no. 20, pp. 4837–4848, 2004, doi: 10.1242/jcs.01370.

[36] G. Bjørkøy *et al.*, “p62/SQSTM1 forms protein aggregates degraded by autophagy and has a protective effect on huntingtin-induced cell death,” *J. Cell Biol.*, vol. 171, no. 4, pp. 603–614, 2005, doi: 10.1083/jcb.200507002.

[37] S. Chen *et al.*, “Targeting SQSTM1/p62 Induces Cargo Loading Failure and Converts Autophagy to Apoptosis via NBK/Bik,” *Mol. Cell. Biol.*, vol. 34, no. 18, pp. 3435–3449, 2014, doi: 10.1128/MCB.01383-13.

[38] T. Johansen and T. Lamark, “Selective autophagy mediated by autophagic adapter proteins,” *Autophagy*, vol. 7, no. 3, pp. 279–296, 2011, doi: 10.4161/auto.7.3.14487.

[39] A. Hamacher-Brady and N. R. Brady, “Mitophagy programs: Mechanisms and physiological implications of mitochondrial targeting by autophagy,” *Cell. Mol. Life Sci.*, vol. 73, no. 4, pp. 775–795, 2016, doi: 10.1007/s00018-015-2087-8.

[40] I. Monastyrska and D. J. Klionsky, “Autophagy in organelle homeostasis: Peroxisome turnover,” *Mol. Aspects Med.*, vol. 27, no. 5–6, pp. 483–494, 2006, doi: 10.1016/j.mam.2006.08.004.

[41] O. S. Shirihai, M. Song, and G. W. Dorn, “How mitochondrial dynamism orchestrates mitophagy.,” *Circ. Res.*, vol. 116, no. 11, pp. 1835–49, May 2015, doi: 10.1161/CIRCRESAHA.116.306374.

[42] R. J. Youle and D. P. Narendra, “Mechanisms of Mitophagy,” *Nature Reviews*, vol. 12. pp. 9–14, 2011.

[43] R. Rojansky, M. Cha, and D. C. Chan, “Elimination of paternal mitochondria in mouse embryos occurs through autophagic degradation dependent on,” *Elife*, vol. 5, pp. 1–18, 2016, doi: 10.7554/eLife.17896.

[44] P. A. Ney, “Mitochondrial autophagy: Origins, significance, and role of BNIP3 and NIX,” *Biochim. Biophys. Acta - Mol. Cell Res.*, vol. 1853, no. 10, pp. 2775–2783, 2015, doi: 10.1016/j.bbamcr.2015.02.022.

[45] H. Sandoval *et al.*, “Essential role for Nix in autophagic maturation of erythroid cells,” *Nature*, vol. 454, no. 7201, pp. 232–235, 2008, doi: 10.1038/nature07006.

[46] W. X. Ding *et al.*, “Nix is critical to two distinct phases of mitophagy, reactive oxygen species-mediated autophagy induction and Parkin-ubiquitin-p62-mediated mitochondrial priming,” *J. Biol. Chem.*, vol. 285, no. 36, pp. 27879–27890, 2010, doi: 10.1074/jbc.M110.119537.

[47] H. Takano-Ohmuro, M. Mukaida, E. Kominami, and K. Morioka, “Autophagy in embryonic erythroid cells: Its role in maturation,” *Eur. J. Cell Biol.*, vol. 79, no. 10, pp. 759–764, 2000, doi: 10.1078/0171-9335-00096.

[48] C. T. Chu, “A pivotal role for PINK1 and autophagy in mitochondrial quality control: implications for Parkinson disease,” vol. 19, no. 1, pp. R28–R37, 2010, doi: 10.1093/hmg/ddq143.

[49] R. K. Dagda, S. J. Cherra, S. M. Kulich, A. Tandon, D. Park, and C. T. Chu, “Loss of PINK1 function promotes mitophagy through effects on oxidative stress and mitochondrial fission,” *J. Biol. Chem.*, vol. 284, no. 20, pp. 13843–13855, 2009, doi: 10.1074/jbc.M808515200.

[50] G. Arena *et al.*, “PINK1 protects against cell death induced by mitochondrial depolarization, by phosphorylating Bcl-xL and impairing its pro-apoptotic cleavage,” *Cell Death Differ.*, vol. 20, no. 7, pp. 920–930, 2013, doi: 10.1038/cdd.2013.19.

[51] E. Barbieri *et al.*, “Mitohormesis in muscle cells: a morphological, molecular, and proteomic approach.,” *Muscles. Ligaments Tendons J.*, vol. 3, pp. 254–66, 2013, doi: 10.11138/mltj/2013.3.4.254.

[52] O. Yamaguchi, T. Murakawa, K. Nishida, and K. Otsu, “Receptor-mediated mitophagy,” *J. Mol. Cell. Cardiol.*, vol. 95, pp. 50–56, 2016, doi: 10.1016/j.yjmcc.2016.03.010.

[53] H. Wei, L. Liu, and Q. Chen, “Selective removal of mitochondria via mitophagy:

Distinct pathways for different mitochondrial stresses," *Biochim. Biophys. Acta - Mol. Cell Res.*, vol. 1853, no. 10, pp. 2784–2790, 2015, doi: 10.1016/j.bbamcr.2015.03.013.

[54] K. E. Liu and W. A. Frazier, "Phosphorylation of the BNIP3 C-terminus inhibits mitochondrial damage and cell death without blocking autophagy," *PLoS One*, vol. 10, no. 6, pp. 1–28, 2015, doi: 10.1371/journal.pone.0129667.

[55] A. B. Birgisdottir *et al.*, "The LIR motif - crucial for selective autophagy.," *J. Cell Sci.*, vol. 126, no. Pt 15, pp. 3237–47, 2013, doi: 10.1242/jcs.126128.

[56] S. M. Jin, M. Lazarou, C. Wang, L. A. Kane, D. P. Narendra, and R. J. Youle, "Mitochondrial membrane potential regulates PINK1 import and proteolytic destabilization by PARL," *J. Cell Biol.*, vol. 191, no. 5, pp. 933–942, 2010, doi: 10.1083/jcb.201008084.

[57] N. Matsuda *et al.*, "PINK1 stabilized by mitochondrial depolarization recruits Parkin to damaged mitochondria and activates latent Parkin for mitophagy," *J. Cell Biol.*, vol. 189, no. 2, pp. 211–221, 2010, doi: 10.1083/jcb.200910140.

[58] E. M. Valente *et al.*, "Hereditary Early-Onset Parkinson's Disease Caused by Mutations in PINK1," *Sci*, vol. 304, no. 5674, pp. 1158–1160, 2004.

[59] T. Kitada *et al.*, "Mutations in the parkin gene cause autosomal recessive juvenile parkinsonism," *Nature*, vol. 392, no. 6676, pp. 605–608, 1998, doi: 10.1038/33416.

[60] D. Narendra, A. Tanaka, D.-F. Suen, and R. J. Youle, "Parkin is recruited selectively to impaired mitochondria and promotes their autophagy," *J. Cell Biol.*, vol. 183, no. 5, pp. 795–803, Dec. 2008, doi: 10.1083/jcb.200809125.

[61] G. Ashrafi and T. L. Schwarz, "The pathways of mitophagy for quality control and clearance of mitochondria," *Cell Death Differ.*, vol. 20, no. 1, pp. 31–42, 2013, doi: 10.1038/cdd.2012.81.

[62] Y. Kim *et al.*, "PINK1 controls mitochondrial localization of Parkin through direct phosphorylation," *Biochem. Biophys. Res. Commun.*, vol. 377, no. 3, pp. 975–980, 2008, doi: 10.1016/j.bbrc.2008.10.104.

[63] K. Shiba-Fukushima *et al.*, "Phosphorylation of Mitochondrial Polyubiquitin by PINK1 Promotes Parkin Mitochondrial Tethering," *PLoS Genet.*, vol. 10, no. 12, 2014, doi: 10.1371/journal.pgen.1004861.

[64] J. Dan Dunn, L. A. J. Alvarez, X. Zhang, and T. Soldati, "Reactive oxygen species and mitochondria: A nexus of cellular homeostasis," *Redox Biol.*, vol. 6, pp. 472–485, 2015, doi: 10.1016/j.redox.2015.09.005.

[65] H. Zhang *et al.*, "Mitochondrial autophagy is an HIF-1-dependent adaptive metabolic response to hypoxia," *J. Biol. Chem.*, vol. 283, no. 16, pp. 10892–10903, 2008, doi: 10.1074/jbc.M800102200.

[66] H. M. Ni, J. A. Williams, and W. X. Ding, "Mitochondrial dynamics and mitochondrial quality control," *Redox Biol.*, vol. 4, pp. 6–13, 2015, doi: 10.1016/j.redox.2014.11.006.

[67] M. Frank *et al.*, “Mitophagy is triggered by mild oxidative stress in a mitochondrial fission dependent manner,” *Biochim. Biophys. Acta - Mol. Cell Res.*, vol. 1823, no. 12, pp. 2297–2310, 2012, doi: 10.1016/j.bbamcr.2012.08.007.

[68] S. Rikka *et al.*, “Bnip3 impairs mitochondrial bioenergetics and stimulates mitochondrial turnover,” *Cell Death Differ.*, vol. 18, no. 4, pp. 721–731, 2011, doi: 10.1038/cdd.2010.146.

[69] H. Gou *et al.*, “CSFV induced mitochondrial fission and mitophagy to inhibit apoptosis,” *Oncotarget*, vol. 8, no. 24, pp. 39382–39400, 2017, doi: 10.18632/oncotarget.17030.

[70] L. Griparic, N. N. Van Der Wel, I. J. Orozco, P. J. Peters, and A. M. Van Der Bliek, “Loss of the Intermembrane Space Protein Mgm1/OPA1 Induces Swelling and Localized Constrictions along the Lengths of Mitochondria,” *J. Biol. Chem.*, vol. 279, no. 18, pp. 18792–18798, 2004, doi: 10.1074/jbc.M400920200.

[71] A. Olichon *et al.*, “Loss of OPA1 perturbates the mitochondrial inner membrane structure and integrity, leading to cytochrome c release and apoptosis,” *J. Biol. Chem.*, vol. 278, no. 10, pp. 7743–7746, 2003, doi: 10.1074/jbc.C200677200.

[72] B. Westermann, “Mitochondrial membrane fusion,” *Biochim. Biophys. Acta - Mol. Cell Res.*, vol. 1641, no. 2–3, pp. 195–202, 2003, doi: 10.1016/S0167-4889(03)00091-0.

[73] C. R. Chang and C. Blackstone, “Dynamic regulation of mitochondrial fission through modification of the dynamin-related protein Drp1,” *Ann. N. Y. Acad. Sci.*, vol. 1201, pp. 34–39, 2010, doi: 10.1111/j.1749-6632.2010.05629.x.

[74] H.-F. Jheng *et al.*, “Mitochondrial Fission Contributes to Mitochondrial Dysfunction and Insulin Resistance in Skeletal Muscle,” *Mol. Cell. Biol.*, vol. 32, no. 2, pp. 309–319, 2012, doi: 10.1128/MCB.05603-11.

[75] T. Koshiba, S. A. Detmer, J. T. Kaiser, H. Chen, J. M. McCaffery, and D. C. Chan, “Structural basis of mitochondrial tethering by mitofusin complexes,” *Sci*, vol. 305, pp. 858–862, 2004.

[76] D. Bach *et al.*, “Mitofusin-2 determines mitochondrial network architecture and mitochondrial metabolism: A novel regulatory mechanism altered in obesity,” *J. Biol. Chem.*, vol. 278, no. 19, pp. 17190–17197, 2003, doi: 10.1074/jbc.M212754200.

[77] O. M. de Brito and L. Scorrano, “Mitofusin 2 tethers endoplasmic reticulum to mitochondria,” *Nature*, vol. 456, no. 7222, pp. 605–611, 2008.

[78] A. Tanaka *et al.*, “Proteasome and p97 mediate mitophagy and degradation of mitofusins induced by Parkin,” *J. Cell Biol.*, vol. 191, no. 7, pp. 1367–1380, 2010, doi: 10.1083/jcb.201007013.

[79] Y. Chen and G. W. Dorn, “PINK1-Phosphorylated Mitofusin 2 Is a Parkin Receptor for Culling Damaged Mitochondria,” *Sci*, vol. 340, pp. 471–476, 2013.

[80] N. C. Chan *et al.*, “Broad activation of the ubiquitin-proteasome system by Parkin is critical for mitophagy,” *Hum. Mol. Genet.*, vol. 20, no. 9, pp. 1726–1737, 2011,

doi: 10.1093/hmg/ddr048.

[81] E. Ziviani, R. N. Tao, and A. J. Whitworth, “Drosophila Parkin requires PINK1 for mitochondrial translocation and ubiquitinates Mitofusin,” *Proc. Natl. Acad. Sci.*, vol. 107, no. 11, pp. 5018–5023, 2010, doi: 10.1073/pnas.0913485107.

[82] S. Ali and G. P. Mcstay, “Regulation of Mitochondrial Dynamics by Proteolytic Processing and Protein Turnover,” *Antioxidants*, vol. 7, no. 1, p. 15, 2018, doi: 10.3390/antiox7010015.

[83] C. Frezza *et al.*, “OPA1 Controls Apoptotic Cristae Remodeling Independently from Mitochondrial Fusion,” *Cell*, vol. 126, no. 1, pp. 177–189, 2006, doi: 10.1016/j.cell.2006.06.025.

[84] V. Romanello *et al.*, “Mitochondrial fission and remodelling contributes to muscle atrophy,” *EMBO J.*, vol. 29, no. 10, pp. 1774–1785, 2010, doi: 10.1038/emboj.2010.60.

[85] M. E. Gegg, J. M. Cooper, K. Y. Chau, M. Rojo, A. H. V. Schapira, and J. W. Taanman, “Mitofusin 1 and mitofusin 2 are ubiquitinated in a PINK1/parkin-dependent manner upon induction of mitophagy,” *Hum. Mol. Genet.*, vol. 19, no. 24, pp. 4861–4870, 2010, doi: 10.1093/hmg/ddq419.

[86] Y. Sun, A. A. Vashisht, J. Tchieu, J. A. Wohlschlegel, and L. Dreier, “Voltage-dependent anion channels (VDACs) recruit parkin to defective mitochondria to promote mitochondrial autophagy,” *J. Biol. Chem.*, vol. 287, no. 48, pp. 40652–40660, 2012, doi: 10.1074/jbc.M112.419721.

[87] S. R. Yoshii, C. Kishi, N. Ishihara, and N. Mizushima, “Parkin mediates proteasome-dependent protein degradation and rupture of the outer mitochondrial membrane,” *J. Biol. Chem.*, vol. 286, no. 22, pp. 19630–19640, 2011, doi: 10.1074/jbc.M110.209338.

[88] T. Zhang *et al.*, “BNIP3 protein suppresses PINK1 kinase proteolytic cleavage to promote mitophagy,” *J. Biol. Chem.*, vol. 291, no. 41, pp. 21616–21629, 2016, doi: 10.1074/jbc.M116.733410.

[89] K. J. Thomas and M. R. Jacobson, “Defects in Mitochondrial Fission Protein Dynamin-Related Protein 1 Are Linked to Apoptotic Resistance and Autophagy in a Lung Cancer Model,” *PLoS One*, vol. 7, no. 9, 2012, doi: 10.1371/journal.pone.0045319.

[90] P. Fortini *et al.*, “The fine tuning of metabolism, autophagy and differentiation during in vitro myogenesis,” *Cell Death Dis.*, vol. 7, no. 3, pp. 1–12, 2016, doi: 10.1038/cddis.2016.50.

[91] L. A. Sabourin and M. A. Rudnicki, “The molecular regulation of myogenesis,” *Clin. Genet.*, vol. 57, no. 1, pp. 16–25, 2000, doi: 10.1034/j.1399-0004.2000.570103.x.

[92] A. B. Lassar, S. X. Skapek, and B. Novitch, “Regulatory mechanisms that coordinate skeletal muscle differentiation and cell cycle withdrawal,” *Curr Opin Cell Biol*, vol. 6, no. 6, pp. 788–794, 1994, doi: 10.1016/0955-0674(94)90046-9.

[93] M. Karbowski and R. J. Youle, “Dynamics of mitochondrial morphology in healthy cells and during apoptosis,” *Cell Death Differ.*, vol. 10, no. 8, pp. 870–880, 2003, doi: 10.1038/sj.cdd.4401260.

[94] S. Frank *et al.*, “The Role of Dynamin-Related Protein 1, a Mediator of Mitochondrial Fission, in Apoptosis,” *Dev. Cell*, vol. 1, no. 4, pp. 515–525, 2001, doi: 10.1016/S1534-5807(01)00055-7.

[95] G. Szabadkai, A. M. Simoni, M. Chami, M. R. Wieckowski, R. J. Youle, and R. Rizzuto, “Drp-1-dependent division of the mitochondrial network blocks intraorganellar Ca2+ waves and protects against Ca 2+-mediated apoptosis,” *Mol. Cell*, vol. 16, no. 1, pp. 59–68, 2004, doi: 10.1016/j.molcel.2004.09.026.

[96] D. Bloemberg, “Examining Autophagy and Mitophagy as Inducible Mechanisms of Cellular Remodelling,” *UWSpace*, 2017.

[97] A. Cassidy-Stone *et al.*, “Chemical Inhibition of the Mitochondrial Division Dynamin Reveals Its Role in Bax/Bak-Dependent Mitochondrial Outer Membrane Permeabilization,” *Dev. Cell*, vol. 14, no. 2, pp. 193–204, 2008, doi: 10.1016/j.devcel.2007.11.019.

[98] A. Tanaka and R. J. Youle, “A Chemical Inhibitor of DRP1 Uncouples Mitochondrial Fission and Apoptosis,” *Mol. Cell*, vol. 29, no. 4, pp. 409–410, 2008, doi: 10.1016/j.molcel.2008.02.005.

[99] S. W. G. Tait *et al.*, “Resistance to caspase-independent cell death requires persistence of intact mitochondria,” *Dev. Cell*, vol. 18, no. 5, pp. 802–813, 2010, doi: 10.1016/j.devcel.2010.03.014.

[100] L. Yang, P. Li, S. Fu, E. S. Calay, and G. S. Hotamisligil, “Defective hepatic autophagy in obesity promotes ER stress and causes insulin resistance,” *Cell Metab.*, vol. 11, no. 6, pp. 467–478, 2010, doi: 10.1016/j.cmet.2010.04.005.

[101] H. Zhang *et al.*, “A novel fission-independent role of dynamin related protein 1 in cardiac mitochondrial respiration,” *Cardiovasc. Res.*, vol. 113, no. 2, pp. 160–170, 2017, doi: 10.1093/cvr/cvw212.

[102] X. Ma, R. J. Godar, H. Liu, and A. Diwan, “Enhancing lysosome biogenesis attenuates BNIP3-induced cardiomyocyte death,” *Autophagy*, vol. 8, no. 3, pp. 297–309, Mar. 2012, doi: 10.4161/auto.18658.

[103] K. C. Yang *et al.*, “Tumor necrosis factor receptorassociated factor 2 mediates mitochondrial autophagy,” *Circ. Hear. Fail.*, vol. 8, no. 1, pp. 175–187, 2015, doi: 10.1161/CIRCHEARTFAILURE.114.001635.

[104] A. J. Valente, L. A. Maddalena, E. L. Robb, F. Moradi, and J. A. Stuart, “A simple ImageJ macro tool for analyzing mitochondrial network morphology in mammalian cell culture,” *Acta Histochem.*, vol. 119, no. 3, pp. 315–326, 2017, doi: 10.1016/j.acthis.2017.03.001.

[105] C. Schöneich, E. Dremina, N. Galeva, and V. Sharov, “Apoptosis in differentiating C2C12 muscle cells selectively targets Bcl-2-deficient myotubes,” *Apoptosis*, vol. 19, no. 1, pp. 42–57, 2014, doi: 10.1007/s10495-013-0922-7.

[106] E. Smirnova, D. Shurland, S. N. Ryazantsev, and A. M. Van Der Bliek, “A Human Dynamin-related Protein Controls the Distribution of Mitochondria,” vol. 143, no. 2, pp. 351–358, 1998.

[107] D. Bloemberg and J. Quadrilatero, “Mitochondrial pro-apoptotic indices do not precede the transient caspase activation associated with myogenesis,” *Biochim. Biophys. Acta - Mol. Cell Res.*, vol. 1843, no. 12, pp. 2926–2936, 2014, doi: 10.1016/j.bbamcr.2014.09.002.

[108] S. Türkseven and A. Zorzano, “Determination of mitochondrial fragmentation and autophagosome formation in C2C12 skeletal muscle cells,” *Turkish J. Med. Sci.*, vol. 43, no. 5, pp. 775–781, 2013, doi: 10.3906/sag-1206-32.

[109] Y. Miyazono, S. Hirashima, N. Ishihara, J. Kusukawa, K. I. Nakamura, and K. Ohta, “Uncoupled mitochondria quickly shorten along their long axis to form indented spheroids, instead of rings, in a fission-independent manner,” *Sci. Rep.*, vol. 8, no. 1, pp. 1–14, 2018, doi: 10.1038/s41598-017-18582-6.

[110] A. M. van der Bliek, Q. Shen, and S. Kawajiri, “Mechanisms of mitochondrial fission and fusion,” *Cold Spring Harb. Perspect. Biol.*, vol. 5, no. 6, 2013, doi: 10.1101/cshperspect.a011072.

[111] Y. Lee, H.-Y. Lee, R. A. Hanna, and A. B. Gustafsson, “Mitochondrial autophagy by Bnip3 involves Drp1-mediated mitochondrial fission and recruitment of Parkin in cardiac myocytes,” *AJP Hear. Circ. Physiol.*, vol. 301, no. 5, pp. H1924–H1931, 2011, doi: 10.1152/ajpheart.00368.2011.

[112] S. Naeem, Y. Qi, Y. Tian, and Y. Zhang, “NIX compensates lost role of parkin in cd-induced mitophagy in HeLa cells through phosphorylation,” *Toxicol. Lett.*, vol. 326, no. December 2019, pp. 1–10, 2020, doi: 10.1016/j.toxlet.2020.03.001.

[113] G. Chinnadurai, S. Vijayalingam, and S. B. Gibson, “BNIP3 subfamily BH3-only proteins: Mitochondrial stress sensors in normal and pathological functions,” *Oncogene*, vol. 27, pp. S114–S127, 2008, doi: 10.1038/onc.2009.49.

[114] J. M. Jurgensmeier, Z. Xie, Q. Deveraux, L. Ellerby, D. Bredesen, and J. C. Reed, “Bax directly induces release of cytochrome c from isolated mitochondria,” *Proc. Natl. Acad. Sci.*, vol. 95, no. 9, pp. 4997–5002, 1998, doi: 10.1073/pnas.95.9.4997.

[115] A. D. Dam, A. S. Mitchell, and J. Quadrilatero, “Induction of mitochondrial biogenesis protects against caspase-dependent and caspase-independent apoptosis in L6 myoblasts,” *Biochim. Biophys. Acta - Mol. Cell Res.*, vol. 1833, no. 12, pp. 3426–3435, 2013, doi: 10.1016/j.bbamcr.2013.04.014.

[116] J. Ju *et al.*, “Autophagy plays a role in skeletal muscle mitochondrial biogenesis in an endurance exercise-trained condition,” *J. Physiol. Sci.*, vol. 66, no. 5, pp. 417–430, 2016, doi: 10.1007/s12576-016-0440-9.

Appendix

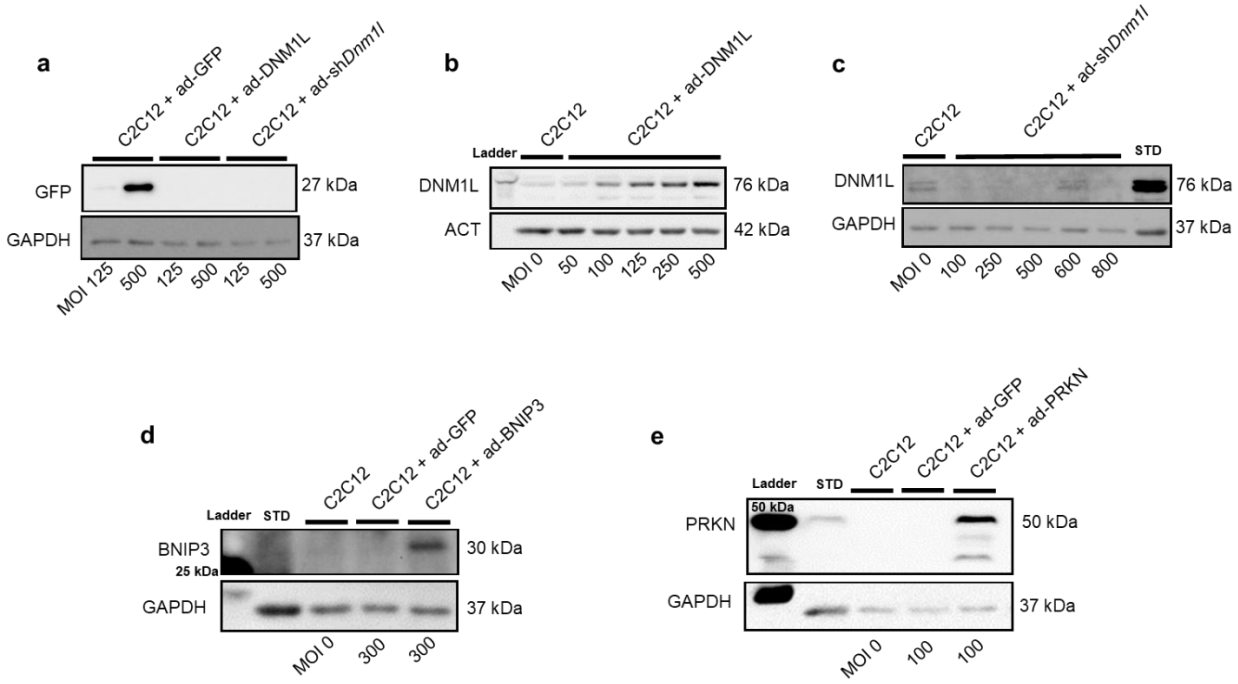

Supplementary Figure 1. Adenoviral vector delivery in C2C12 myoblasts. Representative immunoblots of proliferating (Day 0) C2C12 cells transduced for 24 hours at various multiplicity of infections (MOI) with an adenovirus harbouring constructs for either GFP (**a**), DNM1L (**b**), sh*Dnm1l* (**c**), BNIP3 (**d**), or PRKN (**e**).

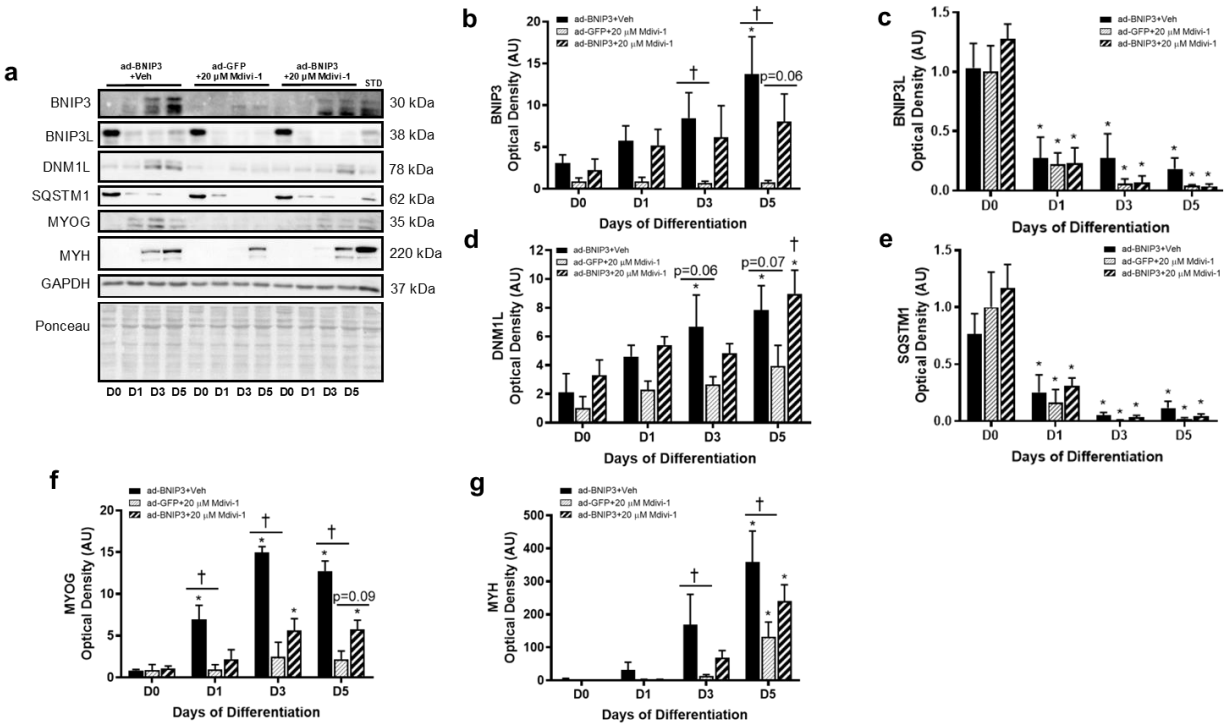

Supplementary Figure 2. BNIP3 overexpression resulted in no impairments in myogenesis and BNIP3 overexpression in differentiated mdivi-1 treated myoblasts upregulated differentiation-related proteins MYOG and MYH. Representative immunoblots (**a**) and quantitative analysis of mitophagy proteins BNIP3 (**b**) and BNIP3L (**c**), mitochondrial fission protein DNM1L (**d**), autophagy-related protein SQSTM1 (**e**), early and late markers of differentiation MYOG (**f**) and MYH (**g**), respectively. *p < 0.05 compared to D0 (within group), †p < 0.05 compared to time-matched ad-GFP+20 μM Mdivi-1 group.

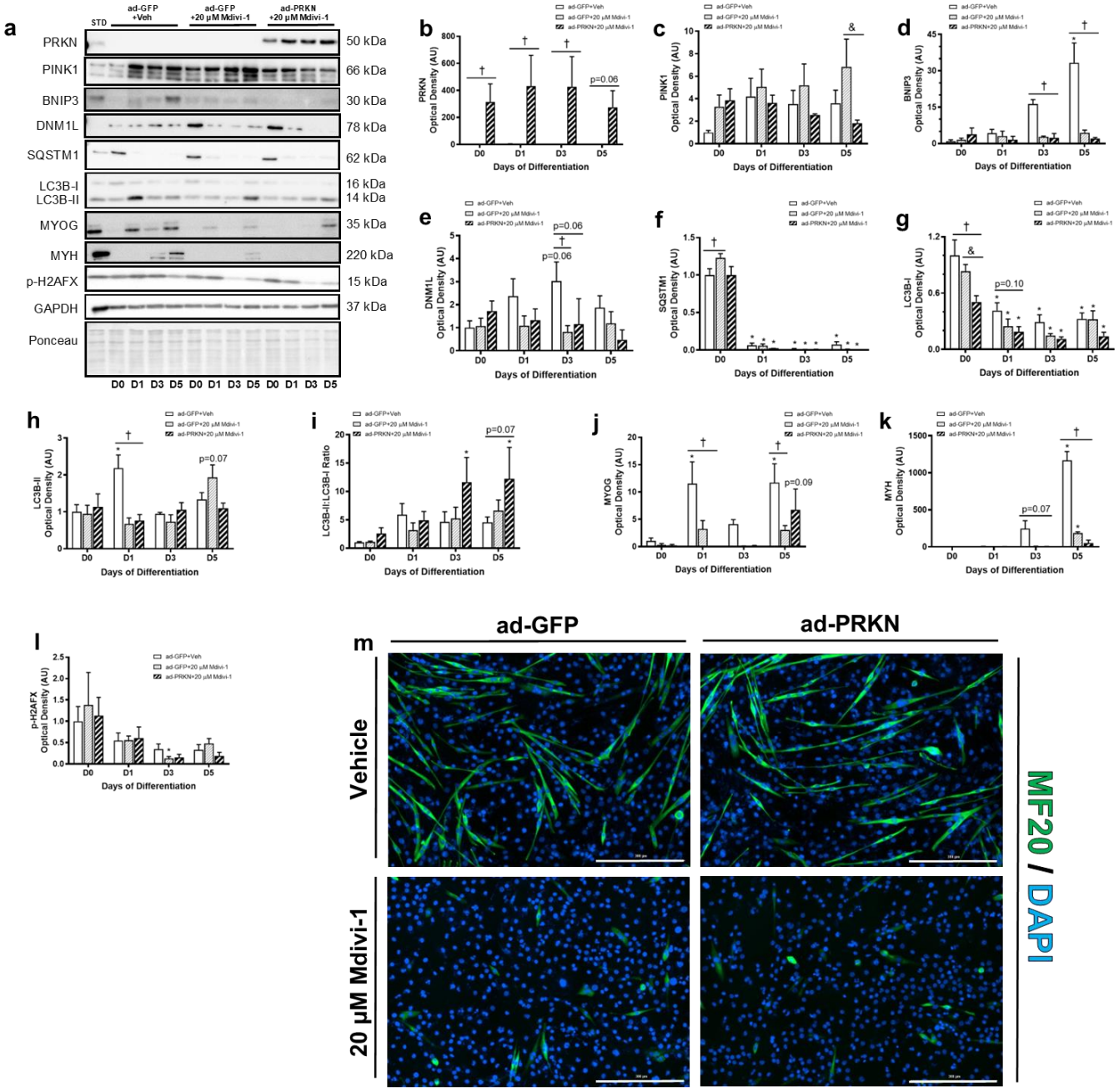

Supplementary Figure 3. PRKN overexpression resulted in no impairments in myogenesis and PRKN overexpression in differentiated mdivi-1 treated myoblasts neither restored the protein levels of differentiation-related proteins MYOG and MYH, nor increased the cell fusion of myoblasts. Representative immunoblots (**a**) and quantitative analysis of mitophagy proteins PRKN (**b**), PINK1 (**c**), and BNIP3 (**d**), mitochondrial fission protein DNM1L (**e**), autophagy-related protein SQSTM1 (**f**), LC3B-I (**g**), LC3B-II (**h**), and calculated LC3B-II:I ratio (**i**), early and late markers of differentiation MYOG (**j**) and MYH (**k**), respectively, and DNA damage marker p-H2AFX (**l**). Representative immunofluorescent images (**m**) of myotube formation in mdivi-1 treated cells at day 5 of differentiation. Cells were stained with DAPI (blue) and for MF20 (green) to visualize nuclei and MYH, respectively. Scale bar = 300 µm. *p < 0.05 compared to D0 (within group), †p < 0.05 compared to time-matched ad-GFP+Veh control group, &p < 0.05 compared to time-matched ad-GFP+20 µM Mdivi-1 group.